AP-1 regulates slow-cycling cells, cellular dormancy and chemoresistance in TNBC

Yang Dong[1,†,$], Jin Bai[2,†], Anmbreen Jamroze[3], Rong Fu[4], Huilan Su[1], Wenwen Xia[5], Shan Wu[1], Ruifang Liu[3], Dean G. Tang[3,*], Jianjun Zhou[1,*]

[1]Research Center for Translational Medicine, Cancer Stem Cell Institute, Shanghai East Hospital, School of Medicine, Tongji University, Shanghai, 200120, China
[2]Department of Oncology, Shanghai East Hospital, School of Medicine, Tongji University, Shanghai, 200120, P.R.China.
[3]Department of Pharmacology and Therapeutics, Roswell Park Comprehensive Cancer Center, Elm and Carlton Streets, Buffalo, NY 14263, USA
[4]Core Facility of Basic Medical Sciences, Basic Medicine Faculty of Shanghai Jiao Tong University School of Medicine, Shanghai 200025, China
[5]Department of Gastroenterology, Shanghai Tenth People's Hospital, School of Medicine, Tongji University, Shanghai 200072, China.

[†]These authors contributed equally to this work.

[$]Current address: Institute of Pathology and Southwest Cancer Center, Southwest Hospital, Third Military Medical University (Army Medical University), ChongQing, 400038, China

*Corresponding authors:

Dean G. Tang (Dean.Tang@Roswellpark.org) or Jianjun Zhou (zhoujj_2000@aliyun.com); Research Center for Translational Medicine, Cancer Stem Cell Institute, Shanghai East Hospital, School of Medicine, Tongji University; 150 Jimo Road, Shanghai, 200120, P.R. China

Key words: triple negative breast cancer, cancer dormancy, activating protein-1, cellular heterogeneity

Running title: AP-1 regulates TNBC slow-cycling cells

Abstract

Background:

Dormant or slow cycling cells (SSCs) pre-exist in tumor and responsible for chemo-resistant and tumor recurrence. Due to their low differentiation and dormancy characteristics, SCCs are resistant to standard chemotherapy and targeted therapy. Label-retaining is a common method used to identify and isolate live SCCs. However, it remains unclear whether different label-retaining methods yield distinct SCC subpopulations. In this study, we investigated that various label-retaining methods result in overlapping yet heterogeneous subpopulations of SCCs. Additionally, we explored the molecular mechanisms regulating dormancy in triple-negative breast cancer (TNBC).

Methods:

We employed multiple label-retaining methods to simultaneously label MDA-MB-231 cells, thereby generating distinct subpopulations of SCCs. We subsequently analyzed these subpopulations for heterogeneity in cell cycle distribution, drug resistance, invasive capacity, and other characteristics using real-time PCR, flow cytometry, and Transwell assays. RNA-seq analysis was performed to characterize the gene expression profiles of the SCCs. Furthermore, we used real-time PCR, Western blotting, immunofluorescence, and luciferase assays to investigate the role of characteristic AP-1 expression in dormancy regulation. Finally, the therapeutic effects of targeting AP-1 in the treatment of TNBC were assessed using a cell-derived xenograft model.

Results:

We labeled and separated three overlapping but non-identical SCCs subpopulations. We found that all three SCCs subgroups are cell cycle arrested. Additionally, Violet enriched SCCs showed stronger drug resistance and more G1 phase arrest, while Claret enriched SCCs demonstrated enhanced migratory and invasive abilities, along with more G2/M phase arrest. Furthermore, we observed upregulation of AP-1 expression in SCCs, and the JunB subunit of AP-1 promoted the expression of CDKN1A and GADD45A, thereby maintaining cell cycle arrest. CC-930 can inhibit AP-1 transcriptional activity by suppressing JNK activity, ultimately improving the therapeutic efficacy and prognosis of TNBC when used in combination with chemotherapy drugs.

Conclusions:

We obtained three subpopulations of SCCs with heterogeneous drug resistance. Our findings suggest that AP-1 plays a regulatory role in dormancy regulation in TNBC, and elucidated the molecular function of JunB subunit. Targeting AP-1 with CC-930 has the potential to improve the treatment and prognosis of TNBC.

1 BACKGROUND

Breast cancer stands as the most prevalent malignancy among women, bearing the highest rates of morbidity and mortality[1]. Among its variants, triple-negative breast cancer (TNBC) presents a challenge in therapy due to the absence of specific markers, resulting in the poorest prognosis and heightened susceptibility to recurrence and metastasis[2]. Currently, clinical treatments predominantly revolve around targeted drugs or anti-mitotic agents. Previous investigations have uncovered the presence of dormant or slow-cycling cells (SCCs) in both autopsy specimens of tumor patients and in vitro cultured cell lines[3,4]. Due to their dormant and poorly differentiated characteristics, these cells exhibit resistance to standard chemotherapy and some targeted therapies. Additionally, certain tumor cells can enter a dormant state in response to drug interventions to evade drug-induced cytotoxicity, known as therapy-induced cells[5]. Both types of cells reside in situ within tumors, forming minimal residual disease. Some cells may undergo a period of dormancy lasting 5 to 10 years before relapsing[6]. Some residual tumor cells migrate into the bloodstream or disseminate to distant organs, termed circulating tumor cells (CTCs) and disseminated tumor cells (DTCs). These cells also exhibit dormancy characteristics, remaining latent within tissues for extended periods and ultimately contributing to tumor recurrence and metastasis[7–10]. Therefore, research targeting dormant tumor cells is crucial for developing more effective treatment strategies. Currently, research on dormancy in TNBC predominantly focuses on DTCs[11–19], while studies related to dormant tumor cells in situ or SCCs remain limited.

The initial identification of SCCs was primarily achieved through Ki67 staining or BrdU chasing[20,21]. However, these methods are mostly destructive and fail to yield live cells for subsequent culture or analysis. Label retention, a widely used technique, enables the isolation of live SCCs and has been extensively utilized in the study of dormant cancer cells in leukemia, melanoma, colorectal cancer, prostate cancer, and breast cancer[22–26]. In this method, cells from tumor tissues or cell lines are uniformly labeled with a fluorescent dye and then subjected to a prolonged chase period. As cells undergo mitosis, the fluorescent label theoretically divides equally between the daughter cells. SCCs retain more fluorescent labels after multiple mitotic cycles, earning them the designation of label-retaining cells (LRCs). Various fluorescent dyes or markers can be employed for label retention (Fig. 1A, B). Pece et al.

utilized the lipophilic fluorescent dye PKH26 to label and isolate human normal mammary stem cells and breast cancer stem cells, noting higher levels of PKH26-retained cells in poorly differentiated tumors compared to well-differentiated tumors[27]. Ebinger et al. labeled patient-derived xenografts of acute lymphoblastic leukemia (ALL) with the protein covalent binding dye CFSE, identifying a rare, long-term dormant cell population resistant to chemotherapy and possessing stem-like properties[28]. Puig et al. adapted a tetracycline-regulated H2B-eGFP fusion protein to label SCCs in colorectal carcinoma, melanoma, and glioblastoma, and further demonstrated the role of TET2 as a key regulator of SCCs in cell number, survival, and tumor recurrence[29]. While label retention methods have been widely employed in the study of adult stem cells or cancer stem cells, there remains a paucity of reports regarding whether different label retention methods yield similar or distinct populations of SCCs. Furthermore, detailed reports on the cellular dormancy mechanisms in breast cancer, particularly triple-negative breast cancer, are still lacking[25,30].

In this study, we employed three distinct label retention methods to simultaneously label MDA-MB-231 cells. Following an extended chase period, we observed overlapping yet non-identical enrichment of slow-cycling cells with different fluorescent labels. We examined the similarities and differences among the three subpopulations of slow-cycling cells from various perspectives, including cell cycle, detoxification, and drug resistance. Subsequently, we conducted RNA-seq analysis to elucidate the source of heterogeneity among the three subpopulations of slow-cycling cells. Our findings revealed that all three subpopulations of slow-cycling cells exhibited overexpression of AP-1-related genes, with this heightened expression correlating with the poor prognosis of TNBC. Through molecular investigations, we identified that JunB overexpression could directly activate the expression of genes such as *CDKN1A* and *GADD45A*, inducing cell cycle arrest and cellular dormancy. Finally, we demonstrated that CC-930, an upstream inhibitor of AP-1, could be combined with chemotherapy drugs to achieve enhanced therapeutic effects.

129 ## 2 METHODS AND MATERIALS

130 ### 2.1 Cell lines and labeling.

131 MDA-MB-231 and SUM159 cells were generous gifts from Dr. Zuoren Yu and. HEK293T cell line was a
132 generous gift from Dr. Ke Wei. All cell lines were identified by STR. MDA-MB-231 cells and HEK293T
133 cells were cultured with high glucose DMEM medium supplied with 10% FBS, SUM159 cells were
134 cultured with RPMI-1640 medium supplied with 10% FBS. For PKH26 (Sigma, #MIDI26, USA) and Claret
135 (Sigma, #MIDCLARET, USA) chasing, cells were washed with PBS 3 times, resuspend with Diluent C
136 solution provided with the kit, and incubated with 10 mM PKH26 dye for 5 minutes at room temperature,
137 protecting from light. Afterwards, cells were washed with Diluent C solution 3 times, and cultured in
138 complete medium. For CFSE (Invitrogen, #C34554, USA) and Violet (Invitrogen, #C34557, USA) chase,
139 cells were washed with PBS once, resuspend with PBS and incubated with 5 mM CellTrace dye for 20
140 minutes at 37 ℃, protecting from light. Afterwards, cells were washed with complete medium twice, then
141 cultured in complete medium. For doxycycline (DOX) chase, cells were treated with 5 mg/ml DOX for at
142 least 3 days in advance, then cultured in DOX-free complete medium. For cells labeled with multiple dyes,
143 perform PKH dyes labeling prior to CellTrace dyes labeling, and culture the labeled cells in DOX-free
144 complete medium (Fig. 1G).

145

146 ### 2.2 Flow cytometry.

147 For fluorescence activated cell sorting (FACS), cells were labeled and chased as previous described. At
148 the end of chasing, cells were collected and DAPI or PI was used to exclude dead cells during sorting.
149 Cells with top 1% fluorescence intensity were sorted as SCCs, cells with moderate fluorescence intensity
150 were sorted as rapid cycling cells (RCCs), and cells without gating on any fluorescence intensity were
151 sorted as bulk control. 1 * 10^5 cells of each subpopulation were sorted and used in subsequent
152 experiments. A Beckman Moflo system was utilized to perform FACS.

153 For flow cytometry analysis, cells were labeled and chased as previous described. PI staining were
154 operated with PI/RNAse staining solution (Invitrogen, #F10797, USA). ALDH activity of each
155 subpopulation was detected by ALDEFLUOR™ Kit (Stemcell, #01700, Canada), and DEAB was used as
156 control. The proportions of senescent cells in each subpopulation were measure by CellEvent™

157 Senescence Green (Invitrogen, #C10841, USA), with cells treated with 1 μM Etoposide as positive control.
158 A Beckman cytoflex system was used to collect the data, and Flow-Jo v10 was used to analysis the data.
159 The t-SNE module was provided by Flow-Jo v10.
160
161 **2.3 Reverse transcription and quantitative PCR.**
162 Total RNA was extracted using Trizol (Invitrogen, #15596018CN, USA) and used to synthesize cDNA
163 using RT reagent Kit with gDNA Eraser, and oligo dT and random hexamer primers were used together
164 (Takara, RR047A, Japan). A Q6 qPCR System was used with TB Green Premix Ex Taq (Takara, RR420A,
165 Japan), and specific pairs of primers (Supplementary Table S1) to detect the indicated transcripts.
166 Relative gene expression was determined by the comparative Ct method.
167
168 **2.4 Immunofluorescence.**
169 Tet-on H2BeGFP stabled transfected cells were cultured with DOX for 3 days, chased in DOX-free
170 medium for 12 days, and fixed with 4% PFA. After fixation, cells were permeabilized with 0.1% Triton X-
171 100 in PBS, followed by 2 washed with PBS and blocked with 4% FBS. Primary antibodies
172 (Supplementary Table S2) were incubated with recommended dilution. Secondary antibody and Hoechst
173 33342 were stained together. Images were collected with ZEISS AX10 system.
174
175 **2.5 Western Blot.**
176 Cells were pelleted and washed once with PBS and resuspended in RIPA lysis buffer supplied with
177 protease inhibitor and phosphatase inhibitor. An ultrasonic device was used to disrupt cells, and lysates
178 were centrifuged to collect supernatants. Protein concentrations were quantified with BCA, and 100μg of
179 each component was loaded. Proteins were separated by SDS-PAGE with 5% spacer gel and 12%
180 separating gel, and later transferred to a PVDF membrane. The membrane was blocked with blocking
181 buffer (LI-COR), and primary antibodies (Supplementary Table S2) were incubated with recommended
182 dilution. IRDye-conjugated secondary antibodies were used, and images were collected with an Odyssey
183 system. All the washes were performed with TBST.
184

185 **2.6 Transwell assay.**

186 Transwell permeable inserts (Corning) were used for migration and invasion analysis. Tri-labeled cells
187 were chased for 12 days, subpopulation of LRCs and ungated bulk cells were sorted by FACS as
188 described above. Cells were washed and resuspended with 200 μl FBS-free DMEM medium and seeded
189 in the upper chamber of inserts with 2.5 * 10^4 cells in each well. The inserts used for invasion analysis
190 were coated with 20μg Matrigel (Corning) in advance. 500 ml complete medium was added to each well
191 of 24-well plate as lower compartment, and the inserts were seated soon after. Continued to culture for
192 24 hours with migration assay, and 48 hours with invasion assay. The inserts were fixed with 1% crystal
193 violet solution for 30 minutes and washed twice with ultrapure water. Cells were counted under
194 microscope with 5 sights for each insert. Images were collected with ZEISS AX10 system.

195

196 **2.7 In vitro chemoresistance.**

197 For in vitro chemoresistance assay, tri-labeled cells were chased for 9 days, and 1μM of each drug
198 (TargetMol.USA) were added. Cells were incubated for 72 hours before fixation and analysis with flow
199 cytometry. For anti-AP1 and TAC combination assays, tri-labeled cells were chased for 9 days prior to
200 drug treatment. A combination of 1.867μM docetaxel, 1.724μM doxorubicin, and 35.829μM
201 cyclophosphamide (TargetMol.USA) was named as TAC. 10μM CC-930 or T-5224 (TargetMol.USA) were
202 used solo or in combination with TAC. Cells were incubated for 72 hours before fixation and analysis with
203 flow cytometry.

204

205 **2.8 Plasmid construction**

206 TetOn-H2BeGFP plasmid (pSIN-TRE-H2BeGFP-hPGK-rtTA2) and fastFUCCI plasmid (pBOB-EF1-
207 FastFUCCI-Puro, Addgene #237968) were acquired from Addgene. pLenti-CMV-MCS-mCherry and pLenti-
208 5'MCS-CMV-mCherry were generous gifts from Dr. Ke Wei. pGL3-basic and pRL-SV40 plasmids were
209 generous gifts from Dr. Yandong Li.

210 For JunB over ovexpression, Homo sapiens JUNB CDS sequence (NCBI Accession No. NM_002229.3) was
211 synthesized and subcloned into multiple cloning sites of pLenti-CMV-MCS-mCherry for lentivirus production.

212 For luciferase assays, AP-1 response element (6x TGAGTCAG) and a minimal TATA-box promoter were

synthesized and cloned into pGL3-basic. This constructed plasmid was named pGL3-AP1re and used to detect AP-1 inhibition activity of CC-903 and T5224. Same synthesized sequence was also cloned into pLenti-5'MCS-CMV-mCherry, replaced whole CMV prompter. Constructed plasmid was named pLenti-AP1re-mCherry and used to trace AP-1 activated cells in vitro.

2 kb upstream of transcription initiation site was considered as promoter region. Promoter region of Homo sapiens CDKN1A (NCBI Gene ID: 1026) and GADD45A (NCBI Gene ID: 1647) were synthesized and cloned into pGL3-basic respectively. Constructed plasmid was named pGL3-pCDKN1A and pGL3-pGADD45A, and used to detect JunB's transcriptional activation of both genes.

All DNA fractions and siRNA were synthesized by Sangon Biotech, Shanghai. All constructs were confirmed by Sanger sequencing.

2.9 Dual luciferase assay.

HEK293T cells were transducted with corresponding plasmids as shown in the illustration with Lipofectamine 2000 (Invitrogen, #11668019, USA). After 72 hours, cells were collected and lysed with Passive Lysis Buffer provided with Dual-Luciferase Reporter Assay System (Promega, #E1910, USA). Both Firefly luciferase activity and Renilla luciferase activity were measured with Glo/Max luminometer following the manual. Relative luciferase activity was calculated using Firefly luciferase luminous intensity / Renilla luciferase luminous intensity (Luc/RLuc) and normalized with control group.

2.10 Colony formation.

500 FACS sorted PKH26^{high} cells or PKH26^{low} cells were plated in 12-well plate and cultured with 500μl complete medium overnight. 1μM CC-930 or equivalent DMSO were added, and half medium were replaced every three days. After 12 days of culture, cells were washed with PBS twice and stained with 1% crystal violet solution for 30 minutes and washed twice with ultrapure water. Images were obtained with Bio-Rad Gel Doc system.

2.11 SA-β-GAL staining.

FACS sorted cells were plated in 4-well chamber slide and cultured overnight. Cells were washed with

241 PBS once and fixed with 500μl β-Galactosidase fixation buffer (Beyotime, #C0602, China). After fixation,
242 cells were washed with PBS for 3 minutes for 3 times, and stained with 500μl mix working staining solution
243 supplied with the kit at 37 ℃ overnight. Images were collected with ZEISS AX10 system.
244
245 **2.12 Tissue microarray (TMA).**
246 TMA (Cat#: TNBC-1202) with 60 paired TNBC samples and adjacent normal tissues were obtained from
247 Shanghai Outdo Biotech, China. Immunohistochemical staining for JunB was performed according to the
248 commercial protocol (Outdo Biotech, Shanghai, China) using anti-JunB antibody (Sigma #HPA019149,
249 USA). The positive proportion of staining was classified as 0, <5%; 1, 5–25%; 2, 25–50%; 3, 50–75%; 4,
250 75–100%. The staining intensity was then classified as 0, negative; 1, weak; 2, moderate; 3, strong. The
251 total score of JunB staining was determined through proportion scores multiplied by intensity scores. The
252 research on the use of human tissue samples was approved by the Medical Ethics Committees of
253 Shanghai East Hospital, Tongji University.
254
255 **2.13 RAN-seq.**
256 Cell were chased and sorted, and RNA was extracted as described above. A total amount of 1μg RNA
257 per sample was used as input material for the RNA sample preparations. Sequencing libraries were
258 generated using NEBNext® UltraTM RNA Library Prep Kit for Illumina® (NEB, USA) following
259 manufacturer's recommendations and index codes were added to attribute sequences to each sample.
260 The clustering of the index-coded samples was performed on a cBot Cluster Generation System using
261 TruSeq PE Cluster Kit v3-cBot-HS (Illumia) according to the manufacturer's instructions. After cluster
262 generation, the library preparations were sequenced on an Illumina Hiseq platform and 125 bp/150 bp
263 paired-end reads were generated.
264
265 **2.14 Survival analysis.**
266 Metadata of clinical outcome and gene expression data was obtained from TCGA-BRCA cohort. Patients
267 were divided into two groups based on gene expression levels. Survival analysis was performed using
268 the survival and survminer packages in R. The Kaplan-Meier method was used to estimate survival

269 functions, and the log-rank test was employed to compare survival curves between groups.

270

271 **2.15 Xenograft model.**

272 1 × 10^6 MDA-MB-231 cells were resuspended with 50μl PBS and 50μl Matrigel and injected into the
273 fourth mammary fat pad on the right flank of female nude mice. When the tumor volume reached
274 approximately 300 mm^3 at approximately 1 week, the mice were randomly assigned into control group,
275 CC-930 group (4 mg/kg), TAC (5 mg/kg/week docetaxel, 3.33 mg/kg/week doxorubicin, and 33.33
276 mg/kg/week cyclophosphamide) group and CC-930 + TAC combination group. CC-930 was given to mice
277 orally, on a daily basis for 21 days. TAC was given to mice i.p. once a week. The tumor volume and body
278 weight were measured three times a week until two days after the final treatment. Tumor volume was
279 calculated as 0.5 × $width^2$ × length. Mice were then sacrificed, and tumors were removed, weighted, and
280 fixed for immunohistochemistry.

281

282 **2.16 Synergy Index Analysis.**

283 Experiments were performed using incremental dosing of each drug for four weeks. For combination
284 studies, the tumor volume data was annotated as viability data and were loaded into the free software
285 Synergy Finder Plus[31]. The software generated surface response plots by comparing the tumor volume
286 inhibition data to a drug combination reference model obtained from the effect of each drug alone.
287 Synergy Finder implemented a bootstrapping method to compare viability data. We considered a *p*-value
288 of less than 0.05 to establish statistical differences between drugs combinations.

289

290 **2.17 Statistical analysis.**

291 Statistical analyses were performed using GraphPad Prism software or using R. In general, student's *t*-
292 test, paired or unpaired two-tailed *t*-test were used to calculate the statistical significance between
293 comparisons depending on the data type. A Chi-square test was performed to calculate the statistical
294 significance of abdominal metastasis incidence. $P<0.05$ is considered statistically significant.

295

296

297 # 3 RESULTS

298 ## 3.1 Different label strategy identified overlapping but not identical slow cycling cells

299 To answer the question whether different label retaining method would result in different LRCs
300 subpopulation, we utilized different fluorescent dyes to label and enrich LRCs. We chose lipophilic dye
301 PKH26 and Claret, and protein affinity dye CFSE and Violet as representatives (Fig. 1A, B). First, MDA-
302 MB-231 cells and SUM159 cells were labeled with these dyes separately. After 12-days of
303 chasing, all four fluorescent dyes were found to be able to label and enrich SCCs (Fig. 1C-F and
304 Supplementary Fig. 1). Next, we labeled MDA-MB-231 cells and SUM159 cell with the four dyes
305 simultaneously and compared SCCs subpopulations with each other. Unsurprisingly, PKH26 label and
306 Claret label had good correlation, even after 12 days of chasing, PKH26 enriched SCCs and Claret
307 enriched SCCs still displayed good correlation. Similar results were also found between CFSE and Violet
308 enriched cells. Nevertheless, the initially observed correlation between cells labeled with disparate dye
309 types diminished rapidly over the course of a 12-day chase, underscoring the existence of heterogeneity
310 among SCCs labeled with diverse dye categories (Supplementary Fig. 2).

311

312 Next, we employed additional fluorescent labeling to isolate a third SCC subpopulation. To this effect,
313 Enhanced Green Fluorescent Protein (eGFP) was fused with Histone 2B and driven by the tetracycline
314 response element. Upon the introduction of doxycycline into the culture environment, the H2B-eGFP
315 fusion protein was expressed, thereby labeling the nuclei[29] (Fig. 1G, H). After a long period of chasing,
316 we identified another subpopulation of SCCs. To investigate the heterogeneity of different SCCs
317 subpopulations, we labeled Tet-on stable transfected MDA-MB-231 cells and SUM159 cells with lipophilic
318 dye Claret and protein affinity dye Violet (Fig. 1I, J). Following a 12-days of chasing, we observed greater
319 overlap between H2B-eGFP-enriched SCCs and Violet-enriched SCCs, with Claret-enriched SCCs
320 demonstrating less overlap with the other two subpopulations (Fig. 1K and Supplementary Fig. 3).
321 Nonetheless, there remained a small population of cells that retained Claret, H2B-eGFP, and Violet labels
322 concurrently, even after the 12-day chase (Fig. 1L). This sparse subpopulation suggested a shared origin
323 among different SCC subpopulations.

324

3.2 Common phenotypes of SCCs: cell cycle arrested and enhanced stemness

Upon identifying three distinct subpopulations of SCCs, we sought to compare and contrast their gene expression profiles and phenotypes. We first examined the cell cycle distribution of those cells. qPCR showed that three subpopulation of SCCs shared similar gene expression pattern of cell cycle related genes. Most cyclin dependent kinases, including *CDK1*, *CDK2* and *CDK6* were down regulated. Most cyclins, including *Cyclin E1*, *Cyclin E2*, *Cyclin A2*, *Cyclin B1* were down regulated as well. Conversely, *CDK4* and *Cyclin D1*, two genes that thought to be involved in G1 cycle arrest[32], had a up regulated tendency. Genes in Cip/Kip family, including *CDKN1A*, *CDKN1B*, *CDKN1C* were obviously up regulated, and *CDKN2C* was down regulated (Fig. 2A). The alterations in Cdk inhibitors (CKIs) expression further confirmed that SCCs were undergoing G0/G1 cell cycle arrest[33]. Cell proliferation associated genes *MKI67* and *PCNA* were down regulated in all three subpopulations of SCCs, and immunofluorescence showed that H2B-eGFP enriched SCCs had lower expression of Ki67 and p-H3 (Fig. 2B), indicating that most of these SCCs were arrested in the G1 phase of mitosis.

We subsequently employed the FastFUCCI system to analyze the cell cycle phase of individual cells. In eukaryotic cells, the licensing factor CDT1 reaches its peak during the G1 phase, subsequently precipitating rapidly in the S phase. Conversely, its inhibitor, Geminin, exhibits heightened expression levels throughout the S and G2 phases, however, it decreases during late mitosis and the G1 phase. These alternating protein expressions are regulated by the alternate activation of E3 ubiquitin ligase SCF^{Skp2} and APC/C^{Cdh1}. Through the Fluorescence ubiquitin cell cycle indicator (FUCCI) technology, the fluorescent proteins mKO and mAG are fused to the destabilized sequences of SCF^{Skp2} and APC/C^{Cdh1} respectively, providing an accurate method to track the cell cycle of individual cells[34,35]. FUCCI analysis revealed that a majority of both Claret-enriched SCCs and Violet-enriched SCCs were arrested in the G1 phase (Fig. 2C). However, unlike each other, a mere 10% of Violet-enriched SCCs entered the S phase or G2/M phase, while nearly 30% of Claret-enriched SCCs transitioned into the S phase and G2/M phase. Based on these findings, we can conclude that these three SCC subpopulations were dormant and arrested within the G1 phase.

353 Furthermore, we examined the association between SCCs and other functional cellular subsets. Firstly,
354 we assessed the detoxification capacity of SCCs using the Aldeflour assay[36]. We found $ALDH^+$ cells to
355 be more prevalent in both Claret and Violet enriched SCCs than in bulk cells. Moreover, they were more
356 abundant in Violet enriched SCCs than in Claret enriched SCCs (Fig. 2E). Next using senescence-
357 associated β-galactosidase (SA-β-GAL) staining, we investigated the link between SCCs and senescent
358 cells. Our analysis revealed few senescent cells in SCCs, signifying that the three SCC subpopulations
359 we identified were not senescent cells with irreversible growth arrest (Supplementary Fig. 4A-C). Then
360 using PI staining, we found a large number of abnormal polyploid cells existed in all three subpopulations
361 of SCCs[37], especially in Violet enriched SCCs (Fig. 2D). We extracted genomic DNA from three
362 subpopulations of SCCs and observed that the Violet-enriched SCCs contained a higher amount of
363 genomic DNA compared to the other subsets (Supplementary Table S3). Finally, we utilized a transwell
364 assay to evaluate the migration and invasion abilities of SCCs. Claret enriched SCCs showed enhanced
365 mobility. While H2B-eGFP and Violet enriched SCCs exhibited higher mobility than bulk cells, although
366 the difference was not statistically significant (Supplementary Fig. 4D, E). Collectively, these data suggest
367 that SCCs from the three subpopulations exhibit similar yet divergent phenotypes.
368

369 **3.3 Different subpopulations of SCCs had diverse chemo-resistance**

370 We subsequently investigated the chemoresistance exhibited by three subpopulations of SCCs to a
371 spectrum of chemotherapeutic drugs. Thirteen chemotherapeutic agents were chosen, falling under three
372 primary categories: taxanes, anthracyclines, and DNA damage agents. These encompass the prevalent
373 drug types utilized in the clinical treatment of TNBC[38,39] (Fig. 3A). We observed distinct drug resistance
374 profiles among the three subpopulations of SCCs after 3 days of treatment. Initially, all three
375 subpopulations of SCCs exhibited resistance to taxanes, with Violet-enriched SCCs demonstrating
376 greater resistance compared to the others (Fig. 3B). Similarly, in contrast to the other subpopulations,
377 H2B-eGFP-enriched SCCs exhibited higher resistance towards anthracyclines (Fig. 3C). Claret-enriched
378 SCCs displayed reduced chemoresistance compared to the other two subpopulations, indicating a lesser
379 detoxification ability. Additionally, SCCs did not exhibit significant enrichment after treatment with PARP
380 inhibitors (Olaparib and Veliparib) and ATR inhibitor AZD6738, whereas significant enrichment was

observed after treatment with ATM inhibitor CP-466722 (Fig. 3D and Supplementary Fig. 5). qPCR analyses indicated suboptimal function in the ATR pathway across all SCC subpopulations, whereas *ATM* and *CHEK2* appeared upregulated (Fig. 3E).

3.4 Enhanced Correlation in Gene Expression Patterns among Different Subpopulations of SCCs

To delve into the heterogeneity among different subpopulations of SCCs, we conducted a comprehensive bulk RNA-seq using each individual population of SCCs along with ungated bulk cells sorted through FACS (Fig. 4A). This analysis showed that the three subpopulations of SCCs were similar regarding their high Pearson correlation coefficient and shared a majority of differentially expressed genes (DEGs, Supplementary Fig. 6B). The GSVA analysis revealed a significant positive correlation of SCCs with the MAPK signaling pathway and PI3K-AKT signaling pathway, contrasted by the negative correlation with DNA replication, DNA damage repair, cell cycle and cell cycle checkpoints (Fig. 4B). The deficiency in these negatively correlated pathways aligns with a dormant phenotype.

We continued our investigation into SCCs' regulatory mechanisms by performing an additional RNA-seq, this time identifying PKH26+ cells as SCCs and PKH26 low cells as controls for rapid cycling cells (RCCs, Fig. 4C). Our findings showed PKH26+ SCCs shared a similar negative correlation with cell cycle, DNA replication, mRNA splicing and ribosome biogenesis. And also we found positive correlation with MAPK pathway and PI3K-AKT activation as previously observed, along with extracellular matrix organization, chemokine signaling and senescence associated secretory phenotype (Fig. 4D, E and Supplementary Fig. 6C). We also identified the AP-1 subunit *FOS* and *FOSB* as the most upregulated DEGs in PKH26^{+} SCCs (Fig. 4F). Furthermore, other subunits of AP-1, namely *JUN*, *JUNB* and *JUND*, were also found upregulated in SCCs (Fig. 4G, H). We finally validated the expression of AP-1 subunits in three subpopulations of SCCs using qPCR (Fig. 4I), deriving that c-Fos family genes *FOS*, *FOSB* as well as c-Jun family genes *JUN*, *JUNB* and *JUND* were upregulated throughout all three subpopulations. Taking the entirety of the data into account, we hypothesize that AP-1 might be a crucial regulator of TNBC cellular dormancy.

409 **3.5 Upregulation of AP-1 subunits in TNBC is a predictor of poor prognosis**

410 To explore the correlation between the expression of AP-1 subunits and the survival of TNBC patients,
411 we categorized the expression levels of AP-1 subunits as high or low using the median gene expression
412 cutoff in the TCGA-BRCA cohort. Initially, we observed that TNBC patients with high expression of FOS
413 or FOSB exhibited worse overall survival (Fig. 5B, C). We further investigated overall breast cancer
414 patients and found no significant difference in overall survival between those with high and low expression
415 of *FOS* or *FOSB*. Considering that ER status is a pivotal factor affecting the survival of BC patients[40],
416 we hypothesized whether the association between high expression of *FOS* or *FOSB* and poor prognosis
417 is related to ER status. Our analysis revealed that high expression of *FOS* or *FOSB* was associated with
418 poor prognosis in ER-negative patients but had no impact on ER-positive patients (Supplementary Fig.
419 7A). Furthermore, we identified a subset of TNBC patients with concurrent high expression of *FOS* and
420 *FOSB*, who exhibited worse prognosis compared to others (Fig. 4D-F). We validated our findings in the
421 METABRIC-TNBC database (Supplementary Fig. 7B). These results indicate that upregulation of *FOS*
422 or *FOSB* serves as a specific predictor of poor prognosis in TNBC.

423

424 **3.6 AP-1 regulate TNBC cellular dormancy and chemo-resistance**

425 To delve deeper into the mechanism by which upregulation of AP-1 subunits affects cellular dormancy,
426 we employed an in vitro chemo-treatment model to investigate whether inhibition of AP-1 could mitigate
427 TNBC's chemo-resistance induced by SCCs. We utilized a combination of docetaxel, doxorubicin, and
428 cyclophosphamide, administered at clinically relevant dosages, which we henceforth refer to as TAC.
429 Following 3 days of TAC treatment, the remaining cells were harvested. We observed an increase in all
430 three subpopulations of SCCs after TAC treatment, with each population expanding from approximately
431 1% to 6.17 ± 0.44%, 50.63 ± 0.80%, and 8.88 ± 0.51%, respectively. Notably, the H2B-eGFP-enriched
432 SCCs exhibited the most prominent increase, suggesting that doxorubicin played a significant role in the
433 enrichment of SCCs. Subsequently, we assessed the efficacy of two AP-1-related small molecule
434 inhibitors: CC-930, a selective c-Jun N-terminal kinase (JNK) inhibitor[41], and T-5224, a c-Fos/c-Jun
435 DNA binding inhibitor[42]. Treating MDA-MB-231 cells with these inhibitors in combination with TAC, we
436 found that CC-930 reduced the enrichment of SCCs resulting from TAC treatment, decreasing to 5.27 ±

437 0.27%, 18.13 ± 0.42%, and 7.74 ± 0.38%, respectively. Conversely, T-5224 did not decrease this
438 enrichment; instead, it increased the populations of H2B-eGFP-enriched and Violet-enriched SCCs to
439 61.90 ± 0.46% and 10.01 ± 0.20% (Fig. 6A and Supplementary Fig. 8). Furthermore, by driving firefly
440 luciferase expression under the AP-1 response element, we established a dual-luciferase assay to
441 measure AP-1 transcriptional activity. After 24 hours of CC-930 treatment, relative firefly luciferase activity
442 decreased, whereas cells treated with T-5224 showed no significant change compared to the control
443 group (Supplementary Figure 9A). Taken together, these data suggest that CC-930 can mitigate the
444 enrichment of SCCs during chemo-treatment by inhibiting AP-1 transcriptional activity.
445
446 We further investigated both gene and protein expression following TAC treatment. qPCR analysis
447 revealed that *FOS* and *FOSB* exhibited the most significant upregulation after TAC treatment, with a
448 32.12-fold change and a 193.50-fold change, respectively. Members of the Jun family, including *JUN*,
449 *JUNB*, and *JUND*, were also upregulated, with *JUNB* showing the highest increase at a 9.54-fold change.
450 Additionally, we examined gene expression changes in the Cip/Kip family and GADD45s. Our findings
451 indicated upregulation of genes associated with AP-1 subunits, the Cip/Kip family, and GADD45s after
452 TAC treatment, which were subsequently reduced upon CC-930 treatment (Fig. 6B). Previous studies
453 have indicated that c-Jun possesses at least two phosphorylation sites, located in both the N-terminal
454 and C-terminal regions. N-terminal phosphorylation enhances c-Jun's transcriptional activity and is
455 mediated by JNK[43]. On the other hand, C-terminal phosphorylation reduces the binding affinity between
456 the c-Jun dimer and DNA, and is catalyzed by GSK3 or CKII, with inhibition via cascade phosphorylation
457 of ERK and p70-S6[44]. In short, both JNK phosphorylation and ERK phosphorylation both contribute to
458 AP-1 transcriptional activity. Therefore, we also performed Western Blot detection on MDA-MB-231 cells
459 treated with TAC or combined with CC-930. We found up-regulation in both JNK and ERK's
460 phosphorylation level after TAC treatment, and could be reversed by CC-930. It's also worth noticing that,
461 although *FOS* and *FOSB* gene expression had most obvious up regulation after TAC treatment, but there
462 was no corresponding increase in protein level. Instead, the protein level of c-Fos, FosB were down
463 regulated after TAC treatment, along with c-Jun (Fig. 6C). Considering the consistency of JunB at both
464 RNA and protein levels, and the contradiction of c-Jun and c-Fos, we hypothesized that among multiple

465 AP-1 subunits, JunB may be the most critical factor regulating dormancy.

466

467 To verify our speculation, we initially observed the co-expression of JunB and other related proteins in
468 SCCs cells. We found co-localization between JunB expression, p21, GADD45A and SCCs marker H2B-
469 eGFP (Fig. 6D). Also, we didn't find much expression of c-Jun in SCCs, which parallels the findings
470 observed in the previous Western blot results. We further developed an additional lentiviral AP-1 reporter
471 system, wherein mCherry expression was driven by the AP-1 response element[45]. Stable MDA-MB-
472 231 cells transfected with this construct were labeled with Claret, H2B-eGFP, and Violet as previously
473 described, and then subjected to a 12-day chase period. Following the chase, the AP-1 transcriptional
474 activity in each subpopulation of SCCs was assessed based on the intensity of mCherry fluorescence.
475 We not only observed stronger AP-1 transcriptional activity in SCCs but also found variations in AP-1
476 transcriptional activity among different subpopulations of SCCs. Specifically, mCherry fluorescence
477 intensity was most pronounced and specific in Violet-enriched SCCs, followed by H2B-eGFP-enriched
478 SCCs and Claret-enriched SCCs (Fig. 6F). Immunofluorescence analysis further confirmed the co-
479 localization between AP-1-derived mCherry expression and H2B-eGFP (Fig. 6E). Importantly, despite
480 minimal differences in AP-1 expression levels, there was significant variability in AP-1 function among the
481 three subpopulations of SCCs. Collectively, these findings underscore the involvement of AP-1 in the
482 regulation of cellular dormancy in TNBC, suggesting that inhibition of AP-1 could effectively disrupt the
483 dormant state of SCCs.

484

485 **3.7 JUNB regulate TNBC cellular dormancy by directly activating the gene expression of CDKN1A**
486 **and GADD45A**

487 To comprehend the specific mechanism by which JunB regulates dormancy, we conducted subsequent
488 experiments. Initially, a paired TMA experiment was performed to investigate JunB expression in patients
489 with TNBC. Our findings revealed significantly higher JunB expression in the TNBC tumor group
490 compared to the tumor adjacent group (Fig. 7A, B). In the subsequent steps, given the transcriptional
491 activity of AP-1, we explored whether JunB could directly activate the expression of genes related to
492 dormancy. We extracted promoter region sequences of the Cip/Kip family and GADD45s and analyzed

493 them using the JASPAR database[46]. Our analysis indicated the presence of AP-1 binding sites in the
494 promoter region of both the Cip/Kip family and GADD45s, with higher affinity observed on both the
495 *CDKN1A* and *GADD45A* promoters (Fig. 7C and Supplementary Table S4). We then constructed another
496 dual-luciferase assay by driving firefly luciferase expression under either the *CDKN1A* promoter or
497 *GADD45A* promoter. We compared the relative firefly luciferase activity when transfected with either the
498 JunB overexpression vector or the control vector. A higher relative firefly luciferase activity was observed
499 when the JunB overexpression vector was transfected, indicating that high levels of JunB directly
500 activated the transcription of either *CDKN1A* or *GADD45A* (Supplementary Fig. 9B). Furthermore, when
501 the JunB overexpression vector was co-transfected with the previously constructed AP-1 response dual-
502 luciferase system, we observed stronger relative firefly luciferase activity, indicating that overexpression
503 of JunB could initiate AP-1 transcription (Supplementary Fig. 9C).
504
505 To confirm the regulatory role of JunB on CDKN1A and GADD45A, we established a stable MDA-MB-
506 231 cell line overexpressing JunB. We observed upregulation of gene expression levels of *JUNB*, *FOS*,
507 *FOSB*, *CDKN1A*, and *GADD45A* in JunB overexpression cells (Fig. 7D). Western blot analysis confirmed
508 the upregulation of p21 and GADD45A in JunB overexpression cells, along with increased levels of
509 phosphorylated ERK1/2 (Fig. 7E). Subsequently, we synthesized two siRNAs targeting JUNB and
510 transfected them into MDA-MB-231 cells, observing an opposite gene expression pattern compared to
511 JunB overexpression. Specifically, AP-1 subunits *FOS*, *FOSB*, and *JUN* were downregulated, while
512 *CDKN1A*, *CDKN1B*, *GADD45A*, and *GADD45B* were also downregulated (Fig. 7F). These findings
513 suggest that the c-Jun/JunB heterodimer can transcriptionally activate the Cip/Kip family and GADD45s.
514 Taken together, all these data support the conclusion that upregulation of JunB in SCCs is a major factor
515 contributing to cellular dormancy.
516
517 **3.8 CC-930 could reduce SCCs residual after chemotherapy in vivo**
518 To investigate the potential of anti-SCC therapy for clinical TNBC treatment, we evaluated CC-930's anti-
519 tumor efficacy both in vitro and in vivo. Previous experiments demonstrated that CC-930 reduced the
520 residual SCCs after chemotherapy. In the colony formation assay, SCCs exhibited higher colony

521 formation capacity than bulk cells, and CC-930 reduced colony formation (Supplementary Fig. 10C).

522

523 Further investigating CC-930's anti-SCCs activity in vivo, we established 40 CDX models with MDA-MB-
524 231 cells. Nude mice bearing CDX were randomly divided into four groups: control, CC-930 treatment,
525 TAC treatment, or TAC + CC-930 combination for 21 days. Initially, tumors treated with TAC shrank but
526 relapsed after 14 days. CC-930 treatment alone showed limited anti-tumor capacity but was effective
527 when combined with TAC. The combination significantly reduced tumor size and weight, preventing tumor
528 regrowth (Fig. 8A, B). As treatment progressed, mice in the TAC and combination groups exhibited a
529 tendency of decreased body weight, which was not observed in the CC-930 treatment group
530 (Supplementary Figure 10B). Abdominal metastases occurred in the control group (6 out of 10) and TAC
531 group (6 out of 10), while no tumors in the CC-930 group developed abdominal metastases, with only 1
532 metastasis in the combination group (Fig. 8C). Finally, using SynergyFinder, we calculated that TAC and
533 CC-930 exhibited a significant synergy effect (Fig. 8D). These findings suggest that CC-930 could
534 enhance survival in TNBC patients treated with traditional chemotherapy.

535

536

4 DISCUSSION

Label retention is one of the most commonly used methods for labeling and enriching SCCs, allowing for the capture of live SCCs for subsequent experiments[22–29]. Different labeling methods employ various fluorescent dyes or fluorescent proteins, prompting a natural question: do different labeling methods yield distinct SCC subpopulations? Our chosen fluorescent labels include lipophilic dyes, protein covalent-binding dyes, and chromatin-tagged fluorescent proteins. These substances belong to the most common components in cells-phospholipid bilayers, chromatin, and proteins, respectively[47]. Firstly, we found that the same type of fluorescent labeling enriches highly correlated SCC subgroups. Various labeling retaining methods offer alternative fluorophores, which can be interchanged without additional impact when faced with limited fluorescent channel availability. More importantly, we found that different types of fluorescent labeling tended to enrich overlapping but not entirely identical SCCs. These SCCs exhibit some phenotypic similarities; for instance, they are all in a slow-cycling state and relatively insensitive to chemotherapy drugs, consistent with previous reports. More importantly, we discovered heterogeneity among these three groups of SCCs both at the distribution and functional levels. The SCCs subpopulation enriched with Claret and that enriched with Violet exhibit substantial differences, while the subpopulation enriched with H2B-eGFP falls between them. Violet enriched SCCs exhibit a more dormant phenotype, characterized by increased G1 phase arrest and enhanced drug resistance. In contrast, Claret enriched SCCs display more G2/M phase arrest, accompanied by weaker drug resistance but stronger migratory capabilities. One interpretation is that different subtypes of SCCs are in varying states of epithelial-mesenchymal transition (EMT)[48,49]. Another interpretation is associated with the enrichment of polyploid giant cancer cells (PGCCs) within SCCs.

PGCCs are a distinct subpopulation of cancer cells characterized by their abnormal DNA content, specifically having multiple sets of chromosomes (polyploidy), and unusually large cell size (giant morphology)[50]. These cells often arise from failed or aberrant cell division processes, such as endoreplication, where DNA replication occurs without subsequent cell division, leading to the accumulation of multiple copies of chromosomes within a single cell[51–53]. PGCCs have been observed in various types of cancers and are associated with tumor aggressiveness, resistance to therapy, and

565 increased metastatic potential[53–56]. PGCCs typically exhibit a dormant phenotype, while their derived
566 daughter cells demonstrate highly invasive and migratory characteristics[57]. We identified the presence
567 of PGCCs within SCCs using PI staining (Fig 2D), and further confirmed the existence of PGCCs in SCCs
568 through quantification of genomic DNA content and immunofluorescence analysis (Fig 6D, E). We found
569 that Violet enriched SCCs exhibited the highest proportion of PGCCs, consistent with the abnormal
570 protein accumulation observed in PGCCs. Meanwhile, certain characteristics of Claret enriched SCCs
571 resembled those of daughter cells derived from PGCCs, particularly the enhanced migratory capacity
572 and G2/M phase arrest. Hence, we speculate that the partial reason for the generation of distinct subtypes
573 of SCCs lies in the differential distribution of various substances during the asymmetric division process
574 of PGCCs. And also, the differences observed in drug resistance to chemotherapy among the three
575 subpopulations, particularly the reactions of Violet enriched SCCs and H2B-eGFP enriched SCCs to
576 taxanes and anthracyclines, can be explained by the theory. Taxanes could cause cytokinesis failure, and
577 anthracyclines could cause karyokinesis failure, forming different forms of PGCCs[58,59]. Regarding the
578 lack of enrichment of SCCs in response to PARP inhibitors and ATR inhibitors, it may be attributed to the
579 p53 mutation in MDA-MB-231 cells[60,61], rendering the cells insensitive to these drugs and thus failing
580 to induce significant cytotoxicity[62,63].
581
582 Another focus of this study lies in the analysis of the signaling pathways regulating dormancy in TNBC.
583 Through RNA-seq, we found that SCCs exhibited downregulation in pathways related to cell cycle, DNA
584 replication, and DNA damage repair, while showing upregulation in the MAPK and PI3K pathways, which
585 is consistent with previous reports[64]. We also identified some expression characteristics of SCCs, such
586 as ECM organization, angiogenesis, oxidative stress response, and protein misfolding, which are
587 consistent with previously reported features of dormant cells[15,16,65–67]. It is noteworthy that we
588 discovered that the function of AP-1, particularly the molecular function of JunB, is a key regulatory factor
589 in cell dormancy.
590
591 The AP-1 is mainly composed of the c-Jun and c-Fos families. c-Jun, as the active center of AP-1, can
592 form homodimers and initiate transcription. c-Fos can form heterodimers with c-Jun, and its

593 transcriptional activity is higher than that of c-Jun homodimers. Both c-Jun homodimers and c-Fos/c-Jun
594 heterodimers can promote cell proliferation. JunB and JunD can form heterodimers with c-Jun. The
595 heterodimers formed have a higher DNA affinity compared to c-Fos/c-Jun dimers and can competitively
596 counteract c-Jun-mediated cell proliferation[68–70]. The AP-1 transcription factor has been extensively
597 studied, particularly its crucial role in regulating cell proliferation and survival[71,72]. Additionally,
598 mounting evidence indicates that AP-1 is involved in multiple processes such as inflammation,
599 differentiation, apoptosis, cell migration, and wound healing[68,71,73]. Recently, it has also been
600 discovered that AP-1 supports angiogenesis, thereby enhancing tumors' ability to cope with harsh
601 microenvironments resulting from hypoxia[74,75]. Regarding cellular heterogeneity, recent evidence
602 suggests that AP-1 also exerts a significant influence on the plasticity of tumor cells[76–91]. A most recent
603 study in prostate cancer shows that FOXA2 collaborates with JUN on chromatin to promote
604 transcriptional reprogramming of AP-1 in lineage plastic cancer cells, thereby facilitating transitions
605 between multiple lineages of cellular states[86]. Our research team also investigated the connection
606 between AP-1 and FOX family members in prostate cancer through single-cell chromatin landscapes,
607 identifying them as critical regulatory factors in castration response[80].
608
609 Furthermore, we found that c-Jun/JunB heterodimers can directly activate the transcription of genes such
610 as *CDKN1A* and *GADD45A*, thereby blocking the cell cycle. It is worth noting that we observed both
611 higher RNA and protein levels of JunB in SCCs, while there were discordant RNA and protein levels of
612 c-Jun and c-Fos. We speculate that this is because JunB competes with c-Jun for binding, leading to
613 rapid degradation of c-Fos and FosB, as c-Fos is a highly unstable protein with rapid nuclear-cytoplasmic
614 shuttling[92]. In addition, recent research has shown that at least one of the three known c-Jun E3
615 ubiquitin ligases, Itch, is activated by JNK phosphorylation[93,94]. Elevated levels of Fos and FosB gene
616 expression favor cell re-entry into the cell cycle and proliferation. When the external environment changes,
617 high levels of gene expression can be efficiently translated into proteins, further promoting cell
618 proliferation. These findings suggest that AP-1, especially JunB subunit, is involved in the regulation of
619 TNBC dormancy. It is also noteworthy that this transition process may not only rely on JunB expression.
620 He et al. reported that JunB can form a complex with YAP/TAZ, and JunB has fewer overlapping motifs

621 with the traditional YAP/TAZ downstream TEAD[95]. This is consistent with previous reports that
622 COL17A1 maintains colon cancer stem cell dormancy by inhibiting YAP/TAZ[96]. In addition, AP-1 can
623 also form complex dimers with other bZIP family members, such as the C/EBP family[69,97]. We also
624 found some of the C/EBP family were highly expressed in SCCs (data not shown). These pieces of
625 evidence indicate that the mechanism by which AP-1 regulates dormancy could be more complex than
626 we described.
627
628 Finally, we discovered that CC-930 sensitizes SCCs to chemotherapeutic drugs by inhibiting AP-1 activity.
629 When used alone, CC-930 did not exhibit significant tumor suppressive effects. However, it effectively
630 prevented abdominal metastases and reduced abdominal metastases induced by TAC treatment in
631 combination groups. It is noteworthy that CC-930 is a safe, orally active drug[41]. The dosage of CC-930
632 used in our study was relatively low compared to other in vivo assays published previously[98–100]. It is
633 possible that a higher dose of CC-930 could yield better results. These findings underscore the potential
634 of anti-SCCs therapy to enhance survival in TNBC patients and highlight CC-930 as an effective
635 treatment option for SCCs.
636
637 Our study also has several limitations. Firstly, our research focuses primarily on in vitro experiments using
638 MD-MB-231 cells, with fewer in vivo experiments conducted. Indeed, many features observed in SCCs,
639 such as elevated ECM expression and enrichment of aging-associated phenotypes, suggest their
640 potential involvement in altering the tumor immune microenvironment. Our previous work has also
641 confirmed the association of dormancy-related ECM with tumor immune suppression
642 microenvironments[65]. Secondly, we lack more clinically relevant models, such as PDX or organoids.
643 Lastly, the minimal gene expression differences among the three subtypes of SCCs could potentially be
644 further elucidated by integrating data such as ATAC-seq to describe the differentiation processes of SCC
645 subtypes.
646
647 **5 CONCLUSIONS**
648

649 In conclusion, we discovered that different label-retaining methods can label and enrich overlapping but
650 not identical subpopulations of SCCs. These SCCs subpopulations are all cell cycle arrested, but they
651 exhibit heterogeneity in cell cycle distribution, drug resistance, invasive and other aspects. We found that
652 the high expression of AP-1 subunits is a poor prognostic factor specific to TNBC, and the AP-1 subunit
653 JunB plays a crucial role in regulating TNBC dormancy. Intervention of AP-1 function with CC-930 in
654 combination with chemotherapy drugs can reduce tumor mass and decrease abdominal metastasis,
655 showing promising clinical applications.
656

657 **AUTH OR CONTRIBUTIONS**

658 Dean G. Tang, Jianjun Zhou and Yang Dong designed this study. Yang Dong, Jin Bai, Anmbreen Jamroze,
659 Rong Fu, Huilan Su, Shan Wu and Wenwen Xia performed the experiments. Dean G. Tang and Jianjun Zhou
660 supervised the direction of project and interpreted the data. Dean G. Tang and Yang Dong wrote the
661 manuscript. All authors discussed the results and commented on the manuscript.
662

663 **ACKNOWLEDGEMENTS**

664 We thank Dr. Zuoren Yu, Dr Yandong Li and Dr Ke Wei (Shanghai East Hospital, Tongji University) and
665 anonymous reviewers for reading and commenting on the manuscript.
666

667 **CONFLICT OF INTERESTS STATEMENT**

668 The authors declare that they have no competing interests.
669

670 **FUNDING INFORMATION**

671 This study was supported by the Chinese Ministry of Science and Technology (MOST) Grant
672 (2016YFA0101201)
673

674 **ETHICS APPROVAL**

675 The research on the use of human tissue samples was approved by the Medical Ethics Committees of
676 Shanghai East Hospital, Tongji University.

CONSENT FOR PUBLICATION

Not applicable.

DATA AVAILABILITY STATEMENT

The RNA-seq data have been deposited in GEO database under accession code GSE267757 and GSE267759

References

1. Sung H, Ferlay J, Siegel RL *et al.* Global Cancer Statistics 2020: GLOBOCAN Estimates of Incidence and Mortality Worldwide for 36 Cancers in 185 Countries. *CA Cancer J Clin* 2021;**71**:209–49.

~~2. Feng Y, Spezia M, Huang S *et al.* Breast cancer development and progression: Risk factors, cancer stem cells, signaling pathways, genomics, and molecular pathogenesis. *Genes Dis* 2018;**5**:77–106.~~

~~3. Davis JE, Kirk J, Ji Y *et al.* Tumor Dormancy and Slow-Cycling Cancer Cells. *Adv Exp Med Biol* 2019;**1164**:199–206.~~

4. Recasens A, Munoz L. Targeting Cancer Cell Dormancy. *Trends Pharmacol Sci* 2019;**40**:128–41.

5. De Angelis ML, Francescangeli F, La Torre F *et al.* Stem Cell Plasticity and Dormancy in the Development of Cancer Therapy Resistance. *Front Oncol* 2019;**9**:626.

6. Gomis RR, Gawrzak S. Tumor cell dormancy. *Mol Oncol* 2017;**11**:62–78.

7. De Angelis ML, Francescangeli F, La Torre F *et al.* Stem Cell Plasticity and Dormancy in the Development of Cancer Therapy Resistance. *Front Oncol* 2019;**9**:626.

8. Phan TG, Croucher PI. The dormant cancer cell life cycle. *Nat Rev Cancer* 2020;**20**:398–411.

~~9. Gao X, Zhang M, Tang Y *et al.* Cancer cell dormancy: mechanisms and implications of cancer recurrence and metastasis. *OncoTargets Ther* 2017;**10**:5219–28.~~

10. Goddard ET, Bozic I, Riddell SR *et al.* Dormant tumour cells, their niches and the influence of immunity. *Nat Cell Biol* 2018;**20**:1240–9.

11. Marti JLG, Beckwitt CH, Clark AM *et al.* Atorvastatin facilitates chemotherapy effects in metastatic triple-negative breast cancer. *Br J Cancer* 2021;**125**:1285–98.

12. Dashzeveg NK, Jia Y, Zhang Y *et al.* Dynamic Glycoprotein Hyposialylation Promotes Chemotherapy Evasion

and Metastatic Seeding of Quiescent Circulating Tumor Cell Clusters in Breast Cancer. *Cancer Discov* 2023;**13**:2050–71.

13. Sunderland A, Williams J, Andreou T *et al.* Biglycan and reduced glycolysis are associated with breast cancer cell dormancy in the brain. *Front Oncol* 2023;**13**:1191980.

14. McGrath J, Panzica L, Ransom R *et al.* Identification of Genes Regulating Breast Cancer Dormancy in 3D Bone Endosteal Niche Cultures. *Mol Cancer Res MCR* 2019;**17**:860–9.

~~15. Farino CJ, Pradhan S, Slater JH. The Influence of Matrix-Induced Dormancy on Metastatic Breast Cancer Chemoresistance. *ACS Appl Bio Mater* 2020;**3**:5832–44.~~

~~16. Farino Reyes CJ, Pradhan S, Slater JH. The Influence of Ligand Density and Degradability on Hydrogel Induced Breast Cancer Dormancy and Reactivation. *Adv Healthc Mater* 2021;**10**:e2002227.~~

17. Payne RE, Hava NL, Page K *et al.* The presence of disseminated tumour cells in the bone marrow is inversely related to circulating free DNA in plasma in breast cancer dormancy. *Br J Cancer* 2012;**106**:375–82.

18. Clark AM, Heusey HL, Griffith LG *et al.* IP-10 (CXCL10) Can Trigger Emergence of Dormant Breast Cancer Cells in a Metastatic Liver Microenvironment. *Front Oncol* 2021;**11**:676135.

19. Shor RE, Dai J, Lee S-Y *et al.* The PI3K/mTOR inhibitor Gedatolisib eliminates dormant breast cancer cells in organotypic culture, but fails to prevent metastasis in preclinical settings. *Mol Oncol* 2022;**16**:130–47.

20. Naumov GN, MacDonald IC, Weinmeister PM *et al.* Persistence of solitary mammary carcinoma cells in a secondary site: a possible contributor to dormancy. *Cancer Res* 2002;**62**:2162–8.

21. Li L, Clevers H. Coexistence of quiescent and active adult stem cells in mammals. *Science* 2010;**327**:542–5.

22. Zhang D, Jeter C, Gong S *et al.* Histone 2B-GFP Label-Retaining Prostate Luminal Cells Possess Progenitor Cell Properties and Are Intrinsically Resistant to Castration. *Stem Cell Rep* 2018;**10**:228–42.

23. Akrap N, Andersson D, Bom E *et al.* Identification of Distinct Breast Cancer Stem Cell Populations Based on Single-Cell Analyses of Functionally Enriched Stem and Progenitor Pools. *Stem Cell Rep* 2016;**6**:121–36.

24. He X, Smith SE, Chen S *et al.* Tumor-initiating stem cell shapes its microenvironment into an immunosuppressive barrier and pro-tumorigenic niche. *Cell Rep* 2021;**36**:109674.

25. Quayle LA, Ottewell PD, Holen I. Chemotherapy resistance and stemness in mitotically quiescent human breast cancer cells identified by fluorescent dye retention. *Clin Exp Metastasis* 2018;**35**:831–46.

26. Xin H-W, Hari DM, Mullinax JE *et al.* Tumor-initiating label-retaining cancer cells in human gastrointestinal cancers undergo asymmetric cell division. *Stem Cells* ~~*Dayt Ohio*~~ 2012;**30**:591–8.

27. Pece S, Tosoni D, Confalonieri S *et al.* Biological and Molecular Heterogeneity of Breast Cancers Correlates with Their Cancer Stem Cell Content. *Cell* 2010;**140**:62–73.

28. Ebinger S, Özdemir EZ, Ziegenhain C *et al.* Characterization of Rare, Dormant, and Therapy-Resistant Cells in Acute Lymphoblastic Leukemia. *Cancer Cell* 2016;**30**:849–62.

29. Puig I, Tenbaum SP, Chicote I *et al.* TET2 controls chemoresistant slow-cycling cancer cell survival and tumor recurrence. *J Clin Invest* 2018;**128**:3887–905.

30. Quayle LA, Spicer A, Ottewell PD *et al.* Transcriptomic Profiling Reveals Novel Candidate Genes and Signalling Programs in Breast Cancer Quiescence and Dormancy. *Cancers* 2021;**13**:3922.

31. Zheng S, Wang W, Aldahdooh J *et al.* SynergyFinder Plus: Toward Better Interpretation and Annotation of Drug Combination Screening Datasets. *Genomics Proteomics Bioinformatics* 2022;**20**:587–96.

32. Lim S, Kaldis P. Cdks, cyclins and CKIs: roles beyond cell cycle regulation. *Dev ~~Camb Engl~~* 2013;**140**:3079–93.

33. Besson A, Dowdy SF, Roberts JM. CDK inhibitors: cell cycle regulators and beyond. *Dev Cell* 2008;**14**:159–69.

34. Koh S-B, Mascalchi P, Rodriguez E *et al.* Quantitative FastFUCCI assay defines cell cycle dynamics at single-cell level. *J Cell Sci* 2016:jcs.195164.

~~35. Zielke N, Edgar BA. FUCCI sensors: powerful new tools for analysis of cell proliferation: FUCCI sensors. *Wiley Interdiscip Rev Dev Biol* 2015;**4**:469–87.~~

~~36. Ahmed-Laskar A, Younus H. Aldehyde toxicity and metabolism: the role of aldehyde dehydrogenases in detoxification, drug resistance and carcinogenesis. *Drug Metab Rev* 2019;**51**:42–64.~~

37. Mosieniak G, Sliwinska MA, Alster O *et al.* Polyploidy Formation in Doxorubicin-Treated Cancer Cells Can Favor Escape from Senescence. *Neoplasia ~~N Y N~~* 2015;**17**:882–93.

3~~8. Medina MA, Oza G, Sharma A *et al.* Triple-Negative Breast Cancer: A Review of Conventional and Advanced Therapeutic Strategies. *Int J Environ Res Public Health* 2020;**17**:2078.~~

39. Korde LA, Somerfield MR, Carey LA *et al.* Neoadjuvant Chemotherapy, Endocrine Therapy, and Targeted Therapy for Breast Cancer: ASCO Guideline. *J Clin Oncol* 2021;**39**:1485–505.

40. Kast K, Link T, Friedrich K *et al.* Impact of breast cancer subtypes and patterns of metastasis on outcome. *Breast Cancer Res Treat* 2015;**150**:621–9.

~~41. Plantevin-Krenitsky V, Nadolny L, Delgado M *et al.* Discovery of CC-930, an orally active anti-fibrotic JNK inhibitor. *Bioorg Med Chem Lett* 2012;**22**:1433–8.~~

42~~. Ishida M, Ueki M, Morishita J *et al.* T-5224, a selective inhibitor of c-Fos/activator protein-1, improves survival by inhibiting serum high mobility group box-1 in lethal lipopolysaccharide-induced acute kidney injury model. *J Intensive Care* 2015;**3**:49.~~

43. Morton S, Davis RJ, McLaren A *et al.* A reinvestigation of the multisite phosphorylation of the transcription factor c-Jun. *EMBO J* 2003;**22**:3876–86.

44. Meng Q, Xia Y. c-Jun, at the crossroad of the signaling network. *Protein Cell* 2011;**2**:889–98.

45. O'Connell DJ, Kolde R, Sooknah M *et al.* Simultaneous Pathway Activity Inference and Gene Expression Analysis Using RNA Sequencing. *Cell Syst* 2016;**2**:323–34.

46. Fornes O, Castro-Mondragon JA, Khan A *et al.* JASPAR 2020: update of the open-access database of transcription factor binding profiles. *Nucleic Acids Res* 2020;**48**:D87–92.

47. Basu S, Dong Y, Kumar R *et al.* Slow-cycling (dormant) cancer cells in therapy resistance, cancer relapse and metastasis. *Semin Cancer Biol* 2021, DOI: 10.1016/j.semcancer.2021.04.021.

48. Paramanantham A, Jung E-J, Kim H-J *et al.* Doxorubicin-Resistant TNBC Cells Exhibit Rapid Growth with Cancer Stem Cell-like Properties and EMT Phenotype, Which Can Be Transferred to Parental Cells through Autocrine Signaling. *Int J Mol Sci* 2021;**22**:12438.

49. Zhou L, Wang D, Sheng D *et al.* NOTCH4 maintains quiescent mesenchymal-like breast cancer stem cells via transcriptionally activating SLUG and GAS1 in triple-negative breast cancer. *Theranostics* 2020;**10**:2405–21.

50. Saini G, Joshi S, Garlapati C *et al.* Polyploid giant cancer cell characterization: New frontiers in predicting response to chemotherapy in breast cancer. *Semin Cancer Biol* 2022;**81**:220–31.

51. Liu J, Niu N, Li X *et al.* The life cycle of polyploid giant cancer cell and dormancy in cancer: opportunities for novel therapeutic interventions. *Semin Cancer Biol* 2022;**81**:132–44.

52. Mirzayans R, Andrais B, Murray D. Roles of Polyploid/Multinucleated Giant Cancer Cells in Metastasis and Disease Relapse Following Anticancer Treatment. *Cancers* 2018;**10**:118.

53. Alhaddad L, Chuprov-Netochin R, Pustovalova M *et al.* Polyploid/Multinucleated Giant and Slow-Cycling Cancer Cell Enrichment in Response to X-ray Irradiation of Human Glioblastoma Multiforme Cells Differing in Radioresistance and TP53/PTEN Status. *Int J Mol Sci* 2023;**24**:1228.

54. Jiao Y, Yu Y, Zheng M *et al.* Dormant cancer cells and polyploid giant cancer cells: The roots of cancer recurrence and metastasis. *Clin Transl Med* 2024;**14**:e1567.

55. Zhou X, Zhou M, Zheng M *et al.* Polyploid giant cancer cells and cancer progression. *Front Cell Dev Biol* 2022;**10**:1017588.

56. Prunier C, Alay A, van Dijk M *et al.* Breast cancer dormancy is associated with a 4NG1 state and not senescence. *NPJ Breast Cancer* 2021;**7**:140.

57. Liu J, Niu N, Li X *et al.* The life cycle of polyploid giant cancer cells and dormancy in cancer: Opportunities for novel therapeutic interventions. *Semin Cancer Biol* 2022;**81**:132–44.

~~58. Margolis RL, Lohez OD, Andreassen PR. G1 tetraploidy checkpoint and the suppression of tumorigenesis. *J Cell Biochem* 2003;**88**:673–83.~~

59. Delespaul L, Merle C, Lesluyes T *et al.* Fusion-mediated chromosomal instability promotes aneuploidy patterns that resemble human tumors. *Oncogene* 2019;**38**:6083–94.

60. Li R, Sutphin PD, Schwartz D *et al.* Mutant p53 protein expression interferes with p53-independent apoptotic pathways. *Oncogene* 1998;**16**:3269–77.

61. Andreidesz K, Koszegi B, Kovacs D *et al.* Effect of Oxaliplatin, Olaparib and LY294002 in Combination on Triple-Negative Breast Cancer Cells. *Int J Mol Sci* 2021;**22**:2056.

62. Ellisen LW. PARP inhibitors in cancer therapy: promise, progress, and puzzles. *Cancer Cell* 2011;**19**:165–7.

63. Tu X, Kahila MM, Zhou Q *et al.* ATR Inhibition Is a Promising Radiosensitizing Strategy for Triple-Negative Breast Cancer. *Mol Cancer Ther* 2018;**17**:2462–72.

~~64. Gao X, Zhang M, Tang Y *et al.* Cancer cell dormancy: mechanisms and implications of cancer recurrence and metastasis. *OncoTargets Ther* 2017;**Volume 10**:5219–28.~~

65. Dong Y, Bai J, Zhou J. Developing a dormancy-associated ECM signature in TNBC that is linked to immunosuppressive tumor microenvironment and selective sensitivity to MAPK inhibitors. *Heliyon* 2024;**10**:e32106.

66. Li C, Qiu S, Liu X *et al.* Extracellular matrix-derived mechanical force governs breast cancer cell stemness and quiescence transition through integrin-DDR signaling. *Signal Transduct Target Ther* 2023;**8**:247.

67. Baldominos P, Barbera-Mourelle A, Barreiro O *et al.* Quiescent cancer cells resist T cell attack by forming an immunosuppressive niche. *Cell* 2022;**185**:1694-1708.e19.

68. Hess J. AP-1 subunits: quarrel and harmony among siblings. *J Cell Sci* 2004;**117**:5965–73.

69. Shaulian E. AP-1--The Jun proteins: Oncogenes or tumor suppressors in disguise? *Cell Signal* 2010;**22**:894–9.

70. Eferl R, Wagner EF. AP-1: a double-edged sword in tumorigenesis. *Nat Rev Cancer* 2003;**3**:859–68.

71. Shaulian E, Karin M. AP-1 as a regulator of cell life and death. *Nat Cell Biol* 2002;**4**:E131–6.

72. Shaulian E, Karin M. AP-1 in cell proliferation and survival. *Oncogene* 2001;**20**:2390–400.

73. Wagner EF, Eferl R. Fos/AP-1 proteins in bone and the immune system. *Immunol Rev* 2005;**208**:126–40.

74. Folkman J. Angiogenesis and c-Jun. *J Natl Cancer Inst* 2004;**96**:644.

75. Laderoute KR. The interaction between HIF-1 and AP-1 transcription factors in response to low oxygen. *Semin Cell Dev Biol* 2005;**16**:502–13.

76. Durand S, Tang Y, Pommier RM *et al.* ZEB1 controls a lineage-specific transcriptional program essential for melanoma cell state transitions. *Oncogene* 2024;**43**:1489–505.

77. Wollenzien H, Afeworki Tecleab Y, Szczepaniak-Sloane R *et al.* Single-Cell Evolutionary Analysis Reveals Drivers of Plasticity and Mediators of Chemoresistance in Small Cell Lung Cancer. *Mol Cancer Res MCR* 2023;**21**:892–907.

~~78. Zhu M, Huang C, Ma X *et al.* Phthalates promote prostate cancer cell proliferation through activation of ERK5 and p38. *Environ Toxicol Pharmacol* 2018;**63**:29–33.~~

79. Marques C, Unterkircher T, Kroon P *et al.* NF1 regulates mesenchymal glioblastoma plasticity and aggressiveness through the AP-1 transcription factor FOSL1. *eLife* 2021;**10**:e64846.

80. Kirk JS, Wang J, Long M *et al.* Integrated single-cell analysis defines the epigenetic basis of castration-resistant prostate luminal cells. *Cell Stem Cell* 2024:S1934-5909(24)00185-1.

~~81. Hardy K, Wu F, Tu W *et al.* Identification of chromatin accessibility domains in human breast cancer stem cells. *Nucl Austin Tex* 2016;**7**:50–67.~~

82. Emmons MF, Faião-Flores F, Sharma R *et al.* HDAC8 Regulates a Stress Response Pathway in Melanoma to Mediate Escape from BRAF Inhibitor Therapy. *Cancer Res* 2019;**79**:2947–61.

83. Sestito R, Tocci P, Roman C *et al.* Functional interaction between endothelin-1 and ZEB1/YAP signaling regulates cellular plasticity and metastasis in high-grade serous ovarian cancer. *J Exp Clin Cancer Res CR* 2022;**41**:157.

84. Serresi M, Kertalli S, Li L *et al.* Functional antagonism of chromatin modulators regulates epithelial-mesenchymal transition. *Sci Adv* 2021;**7**:eabd7974.

85. Casalino L, Talotta F, Matino I *et al.* FRA-1 as a Regulator of EMT and Metastasis in Breast Cancer. *Int J Mol Sci* 2023;**24**:8307.

86. Wang Z, Townley SL, Zhang S *et al.* FOXA2 rewires AP-1 for transcriptional reprogramming and lineage plasticity in prostate cancer. *Nat Commun* 2024;**15**:4914.

87. Kadur Lakshminarasimha Murthy P, Xi R, Arguijo D *et al.* Epigenetic basis of oncogenic-Kras-mediated epithelial-cellular proliferation and plasticity. *Dev Cell* 2022;**57**:310-328.e9.

88. Ogasawara N, Kano Y, Yoneyama Y *et al.* Discovery of non-genomic drivers of YAP signaling modulating the cell plasticity in CRC tumor lines. *iScience* 2024;**27**:109247.

89. Zhang X, Pant SM, Ritch CC *et al.* Cell state dependent effects of Bmal1 on melanoma immunity and tumorigenicity. *Nat Commun* 2024;**15**:633.

90. Kuonen F, Li NY, Haensel D *et al.* c-FOS drives reversible basal to squamous cell carcinoma transition. *Cell Rep* 2021;**37**:109774.

91. Comandante-Lou N, Baumann DG, Fallahi-Sichani M. AP-1 transcription factor network explains diverse

patterns of cellular plasticity in melanoma cells. *Cell Rep* 2022;**40**:111147.

92. Malnou CE, Salem T, Brockly F *et al.* Heterodimerization with Jun family members regulates c-Fos nucleocytoplasmic traffic. *J Biol Chem* 2007;**282**:31046–59.

93. Gao M, Labuda T, Xia Y *et al.* Jun turnover is controlled through JNK-dependent phosphorylation of the E3 ligase Itch. *Science* 2004;**306**:271–5.

94. Anzi S, Finkin S, Shaulian E. Transcriptional repression of c-Jun's E3 ubiquitin ligases contributes to c-Jun induction by UV. *Cell Signal* 2008;**20**:862–71.

95. He L, Pratt H, Gao M *et al.* YAP and TAZ are transcriptional co-activators of AP-1 proteins and STAT3 during breast cellular transformation. *eLife* **10**:e67312.

96. Ohta Y, Fujii M, Takahashi S *et al.* Cell-matrix interface regulates dormancy in human colon cancer stem cells. *Nature* 2022;**608**:784–94.

97. Hong S, Skaist AM, Wheelan SJ *et al.* AP-1 protein induction during monopoiesis favors C/EBP: AP-1 heterodimers over C/EBP homodimerization and stimulates FosB transcription. *J Leukoc Biol* 2011;**90**:643–51.

98. Velden JLJ, Ye Y, Nolin JD *et al.* JNK inhibition reduces lung remodeling and pulmonary fibrotic systemic markers. *Clin Transl Med* 2016;**5**, DOI: 10.1186/s40169-016-0117-2.

~~99. Reich N, Tomcik M, Zerr P *et al.* Jun N-terminal kinase as a potential molecular target for prevention and treatment of dermal fibrosis. *Ann Rheum Dis* 2012;**71**:737–45.~~

~~100. Yang F, Ozols E, Ma FY *et al.* c-Jun Amino Terminal Kinase Signaling Promotes Aristolochic Acid-Induced Acute Kidney Injury. *Front Physiol* 2021;**12**:599114.~~

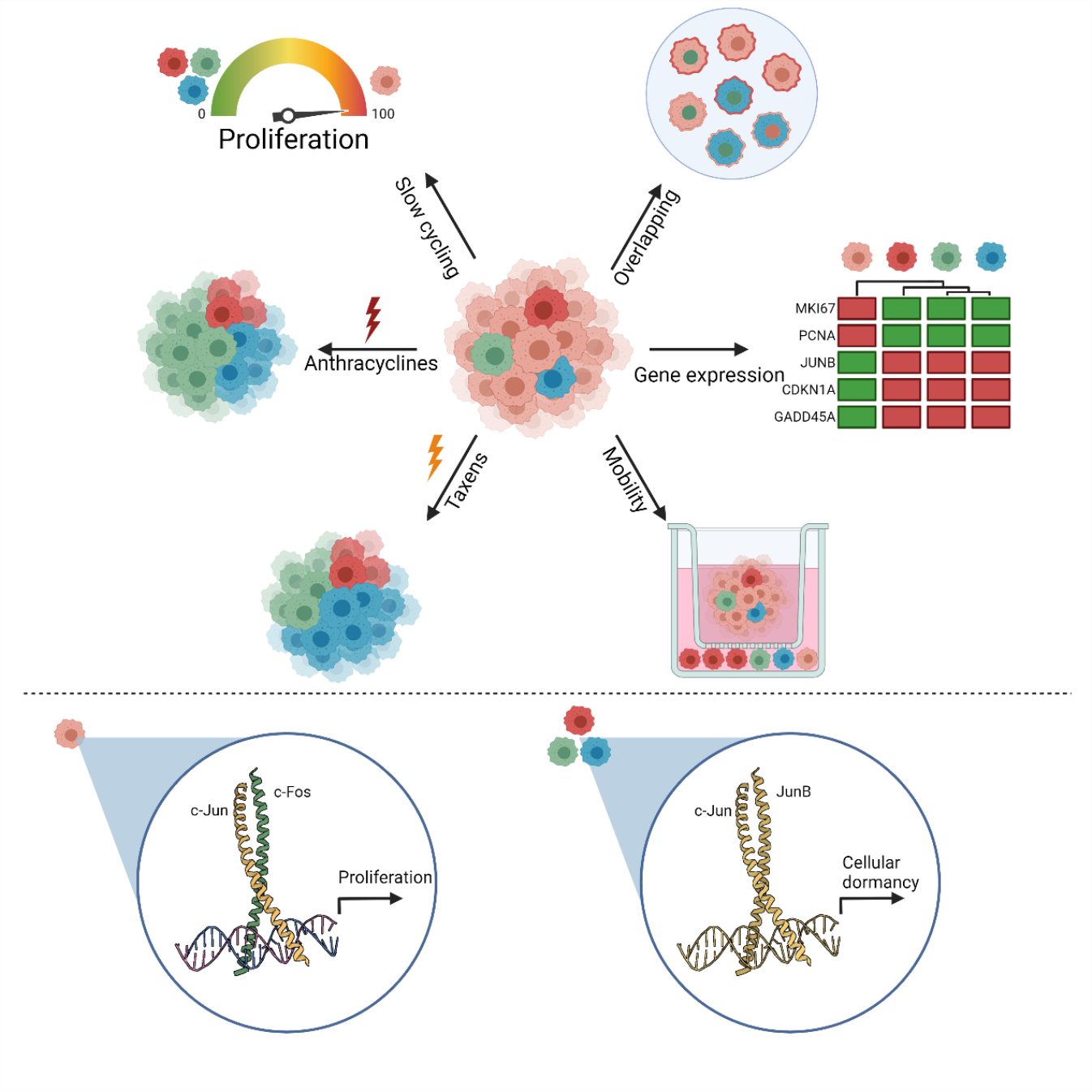

Graphical Abstract

TNBC harbors both fast-cycling cells (FCCs) and functionally overlapping slow-cycling cell (SCC) subpopulations that manifest differential drug sensitivities and motility (A) but are commonly regulated by the JunB-containing AP1 complex (B).

(A). Slow-cycling (quiescent) TNBC cells in culture (a) identified by different label-retaining approaches phenotypically overlap (b), display differential drug sensitivities (c, d) and motility (e) but share common gene expression profiles (f).

888 (B). Schematic depicting regulation of proliferation in FCCs by the c-Jun/c-Fos AP1 complex (left) and
889 regulation of cellular dormancy in SCCs by c-Jun/JunB AP1 complex.
890
891

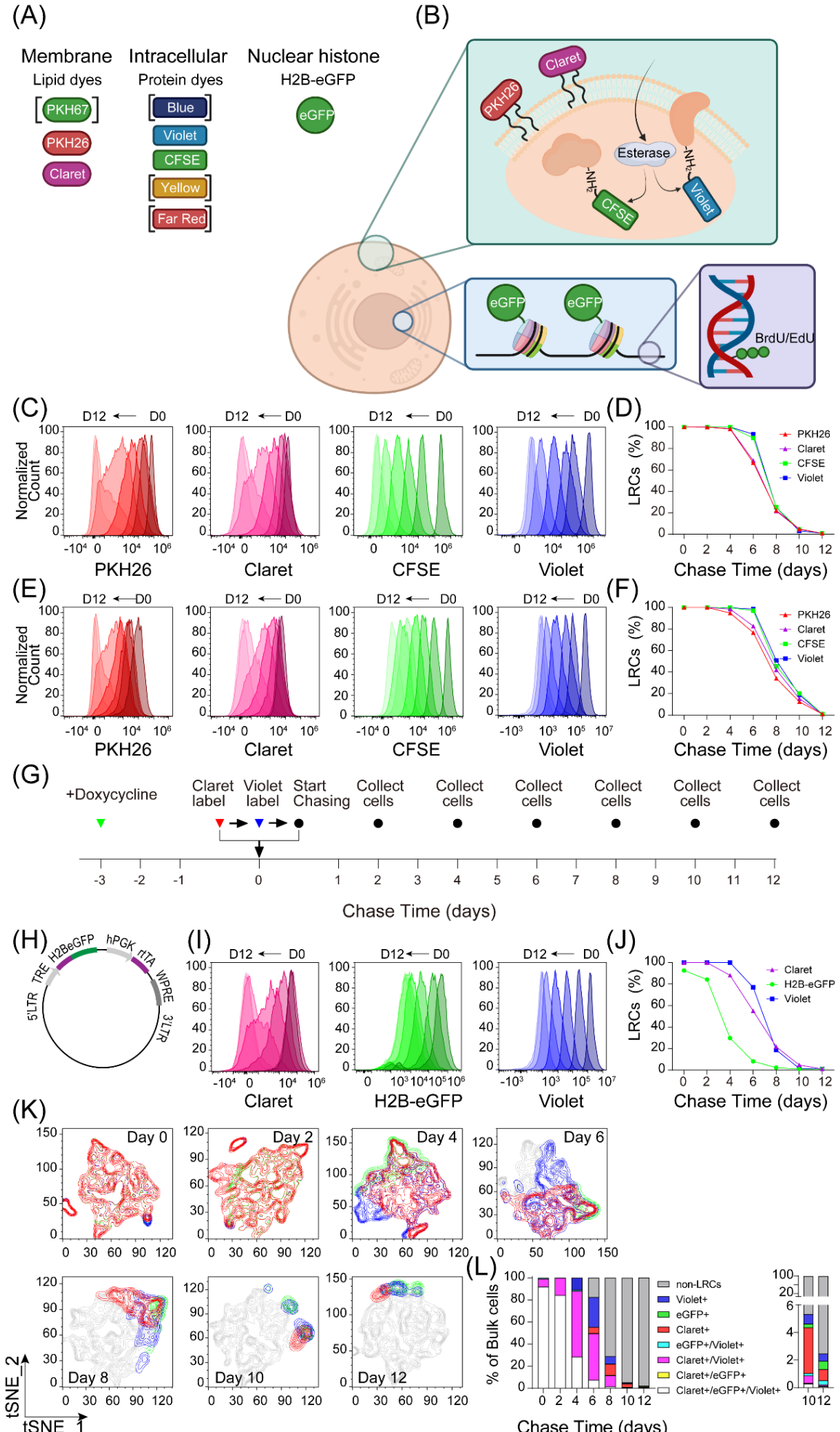
(A)
Membrane
Lipid dyes
PKH67
PKH26
Claret
Intracellular
Protein dyes
Blue
Violet
CFSE
Yellow
Far Red
Nuclear histone
H2B-eGFP
eGFP
(B)
Claret
PKH26
Esterase
CFSE
Violet
eGFP
eGFP
BrdU/EdU
(C)
D12 ← D0
Normalized Count
PKH26
Claret
CFSE
Violet
(D)
LRCs (%)
PKH26
Claret
CFSE
Violet
Chase Time (days)
(E)
(F)
(G)
+Doxycycline
Claret label
Violet label
Start Chasing
Collect cells
Chase Time (days)
(H)
H2BeGFP
hPGK
rtTA
WPRE
3'LTR
5'LTR
TRE
(I)
Claret
H2B-eGFP
Violet
(J)
Claret
H2B-eGFP
Violet
Chase Time (days)
(K)
Day 0
Day 2
Day 4
Day 6
Day 8
Day 10
Day 12
tSNE_1
tSNE_2
(L)
% of Bulk cells
non-LRCs
Violet+
eGFP+
Claret+
eGFP+/Violet+
Claret+/Violet+
Claret+/eGFP+
Claret+/eGFP+/Violet+
Chase Time (days)

Fig 1: Different LRC strategies identify overlapping but non-identical SCC populations.
(A, B) Different labeling methods of SCCs. BrdU/EdU can be incorporated into DNA during S phase instead of thymine. But this method could not label live SCCs for the subsequent experiments. Lipophilic dyes label the phospholipid bilayer of cells through a hydrophobic tail. Protein covalent binding dyes enter the cells by diffusion. The ester group got removed by intracellular esterase, and the fluorescent part of the dye covalently bound to the available amino groups of intracellular protein and intracellular portion of transmembrane protein. eGFP and H2B fusion protein is expressed under the control of tetracycline responding element, thereby traces chromosomes and nucleus. Alternative dyes with different fluorescence are listed on the left. The dyes in parentheses were not used in this study.
(C, D) MDA-MB-231 cells and (E, F) SUM159 cells were labeled with PKH26, Claret, CFSE, and Violet separately. Cells were collected and fixed every other day from day 0 to day 12. Fluorescent intensity of each dye was analyzed by flow cytometry.
(G) Timeline of tri-labeling strategies. Stable transfected MDA-MB-231 cells were cultured with doxycycline for at least 3 days, then claret labeling and violet labeling were accomplished in order. Cells were collected and fixed every other day from day 0 to day 12. Fluorescent intensity of each dye was analyzed by flow cytometry.
(H) Schematics of Tet-On H2B-eGFP expression vector.
(I, J) Label retaining effect of Claret, H2B-eGFP and Violet in tri-labeled cells. MDA-MB-231 cells were labeled following aforementioned timeline. Fluorescent intensity of each dye was analyzed by flow cytometry.
(K) tSNE plot and (L) stacked histogram of each time point.

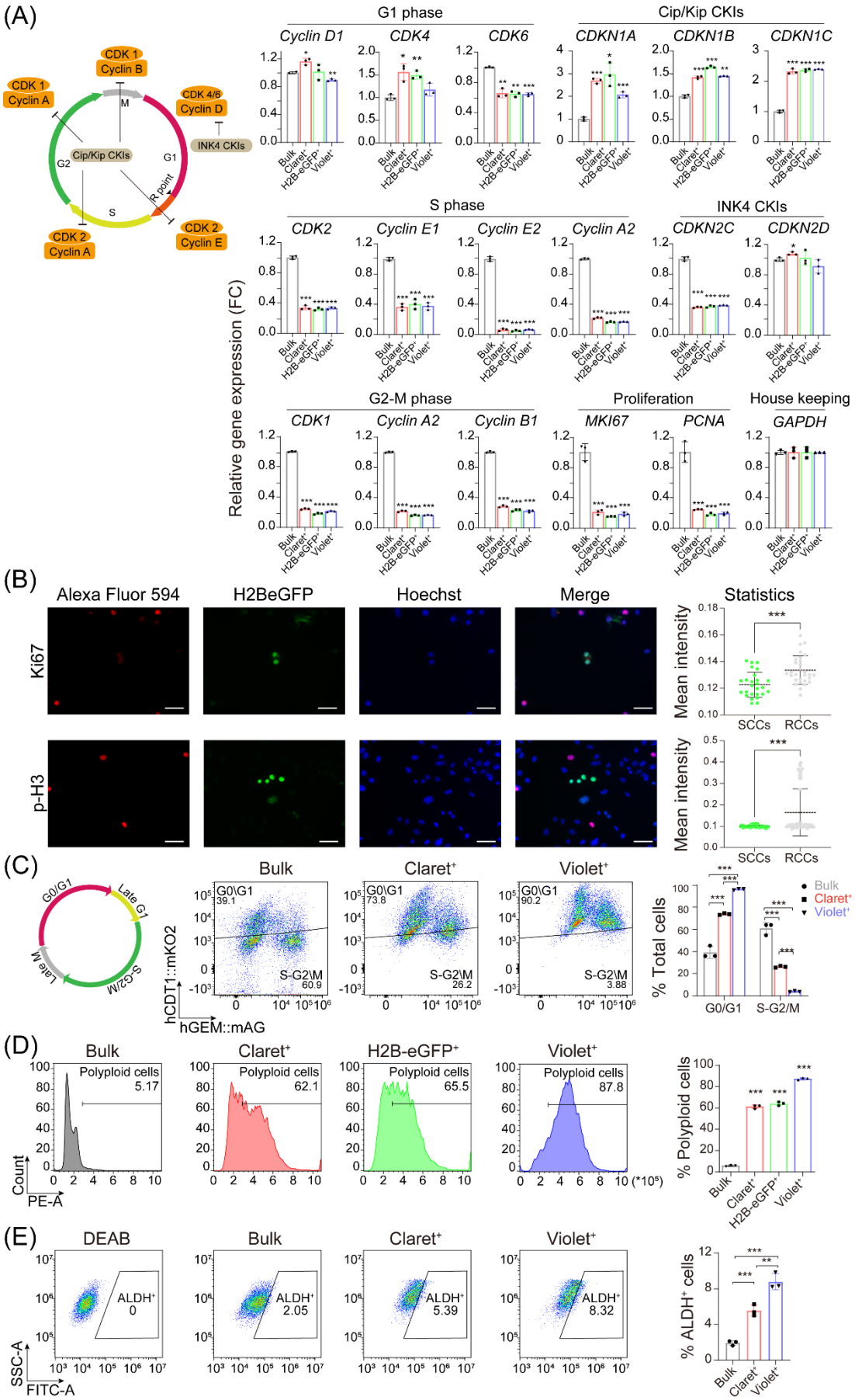

(Dong et al. Fig 2)

916 **Fig 2: Biological and functional properties of SCCs**

917 (A) 3 SCCs populations showed similar gene expression pattern in cell cycle related genes. Tri-labeled MDA-
918 MB-231 cells were chased for 12 days. Each SCCs population was sorted by FACS, and bulk cells were also
919 sorted as control. Relative gene expressions of SCCs and bulk cells were analyzed by RT-qPCR.

920 (B) Immunofluorescence showed H2B-eGFP enriched SCCs had lower expression of p-H3 and Ki67 after 12
921 days of chasing. Tet-On H2B-eGFP transfected MDA-MB-231 cells were incubated with doxycycline for 3 days
922 and chasing without doxycycline for 12 days. Cells were fixed and permeabilized, and stained with
923 corresponding antibody. Scale bar = 20 μm.

924 (C) Cell cycle of each population was monitored by FUCCI. FUCCI transfected MDA-MB-231 cells were
925 labeled with Claret and Violet and chased for 12 days. Equal amount of bulk cells, Claret$^+$ SCCs and Violet$^+$
926 SCCs were collected and cell cycle distributions were analyzed. Claret$^+$ SCCs were spread among different
927 phases, while Violet$^+$ SCCs were mostly arrested in late G1 phase.

928 (D) Polyploid cells were more enriched in SCCs compared with bulk MDA-MB-231 cells. Tri-labeled MDA-MB-
929 231 cells were chased for 12 days. Cells were fixed and stained with PI. Equal amount of bulk cells, Claret$^+$
930 SCCs and Violet$^+$ SCCs were collected and cells DNA content >4N were considered as polyploid cells. Violet$^+$
931 SCCs enriched more polyploid cells then H2B-eGFP$^+$ SCCs and Claret$^+$ SCCs.

932 (E) ALDH$^+$ cells were more enriched in SCCs compared with bulk MDA-MB-231 cells. MDA-MB-231 cells were
933 labeled with Claret and Violet and chased for 12 days. Equal number of bulk cells, Claret$^+$ SCCs and Violet$^+$
934 SCCs were collected and ALDH$^+$ cells were identified by DEAB control. Violet$^+$ SCCs enriched more ALDH$^+$
935 cells then Claret$^+$ SCCs.

936 Data are represented as mean ± SD. *p ≤0.05; **p ≤0.01; ***p ≤0.001, Student's t test.

937

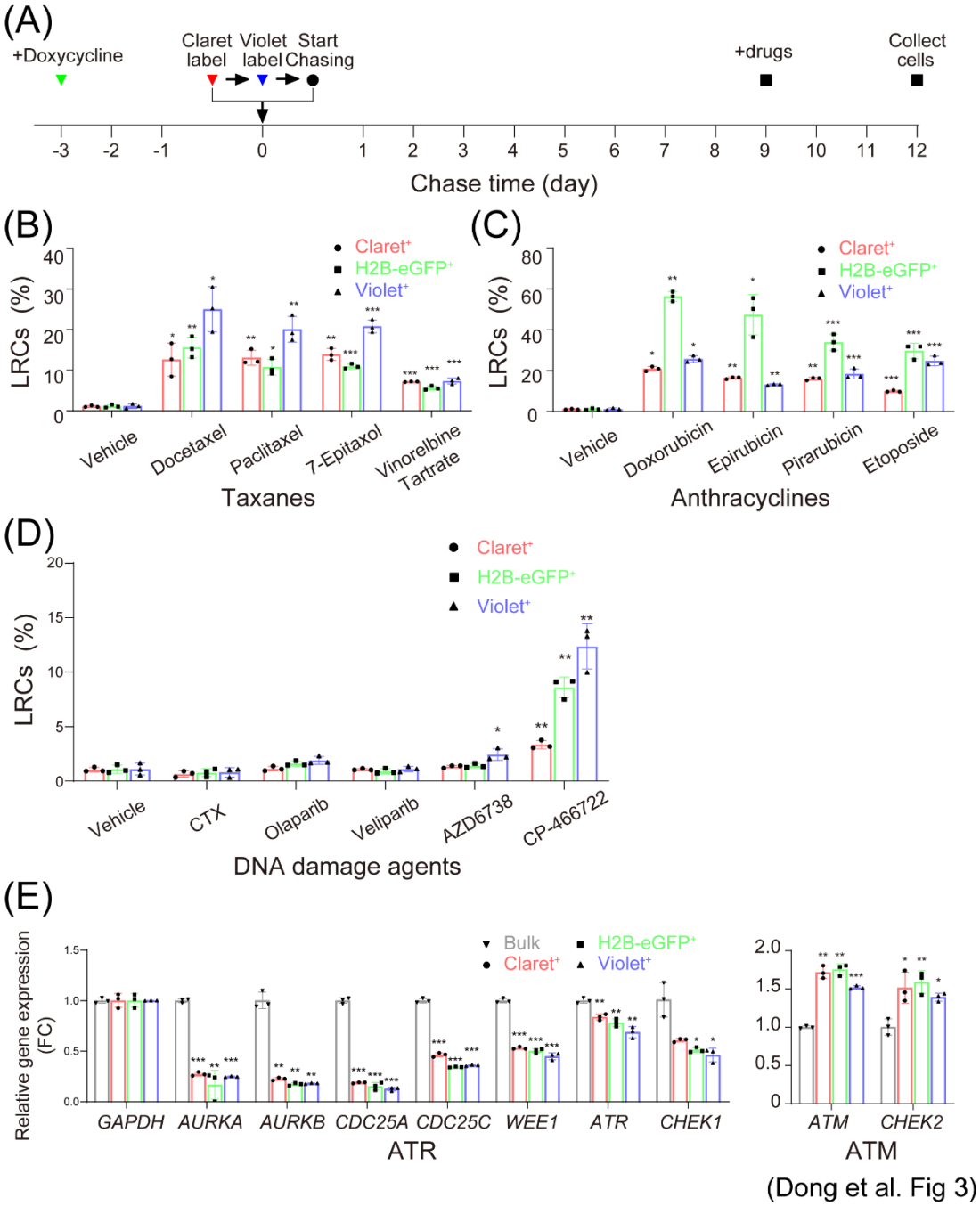

(Dong et al. Fig 3)

Fig 3: Diverse SCCs have different chemotherapeutic tolerances

(A) Timeline of chemo-resistance assay. Tri-labeled MDA-MB-231 were chased for 9 days, and 1 μM each drug was added respectively. After 3 days of culture cells were collected and analyzed with flow cytometry.

(B) More Violet$^+$ SCCs retained after taxane treatment, indicating that Violet$^+$ SCCs were more resistant to taxanes.

(C) More H2B-eGFP$^+$ SCCs retained after anthracycline treatment, indicating that H2B-eGFP$^+$ SCCs were

945 more resistant to anthracyclines.

946 (D) SCCs didn't show significant retaining after PARP inhibitors treatment.

947 (E) SCCs were up-regulated in *ATM* and *CHEK2*, and down-regulated in ATR pathway. Tri-labeled MDA-MB-

948 231 cells were labeled and chased for 12 days. Each SCCs population was sorted by FACS, and bulk cells

949 were also sorted as control. Relative gene expressions of SCCs and bulk cells were analyzed by RT-qPCR.

950 Data are represented as mean ± SD. *p ≤0.05; **p ≤0.01; ***p ≤0.001, Student's t test.

951

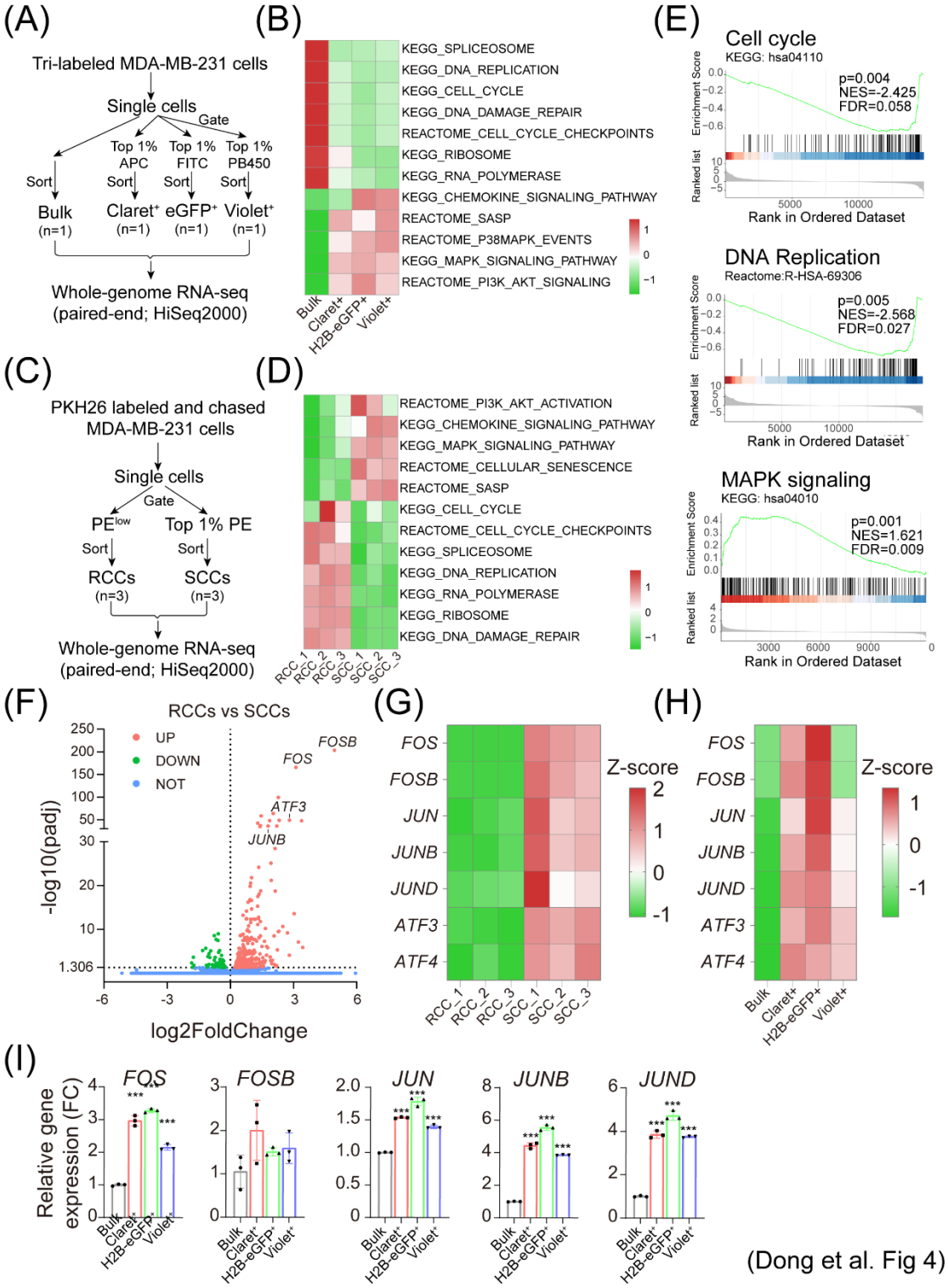

(Dong et al. Fig 4)

Fig 4: RNA-seq reveal SCCs are enriched in AP-1 signaling and anti-stress mechanisms

(A, C) Flow chart of FACS and RNA-seq. Tri-labeled MDA-MB-231 were chased for 12 days. Top 1% of each population were sorted and names as distinct SCCs subpopulation. Meanwhile, cells that were not gated with

956 any fluorescence channel were sorted as Bulk cell control. Each subpopulation was collected for one sample.
957 MDA-MB-231 cells were labeled and chased with PKH26 for 12 days. Top 1% PE^{+} cells were sorted and
958 named as SCCs, and PE^{low} cells were sorted and names as RCCs. Each subpopulation was collected with
959 triple replications.
960 (B, D) GSVA analysis showed similar pathway enrichment in three SCCs subpopulations.
961 (E) GSEA analysis showed MAPK signaling pathway were up-regulated in $PKH26^{+}$ SCCs, and cell cycle and
962 DNA replication associated pathways were down-regulated in $PKH26^{+}$ SCCs.
963 (F) Volcano plot of DEGs in $PKH26^{+}$ SCCs. FOS and FOSB were the most remarkable up-regulations genes.
964 (G, H) Heatmaps of AP-1 subunits' expression in RNA-seq data.
965 (I) AP-1 subunits were up-regulated in SCCs. Tri-labeled MDA-MB-231 cells were labeled and chased for 12
966 days. Each SCCs population was sorted by FACS, and bulk cells were also sorted as control. Relative gene
967 expressions of SCCs and bulk cells were analyzed by RT-qPCR.
968

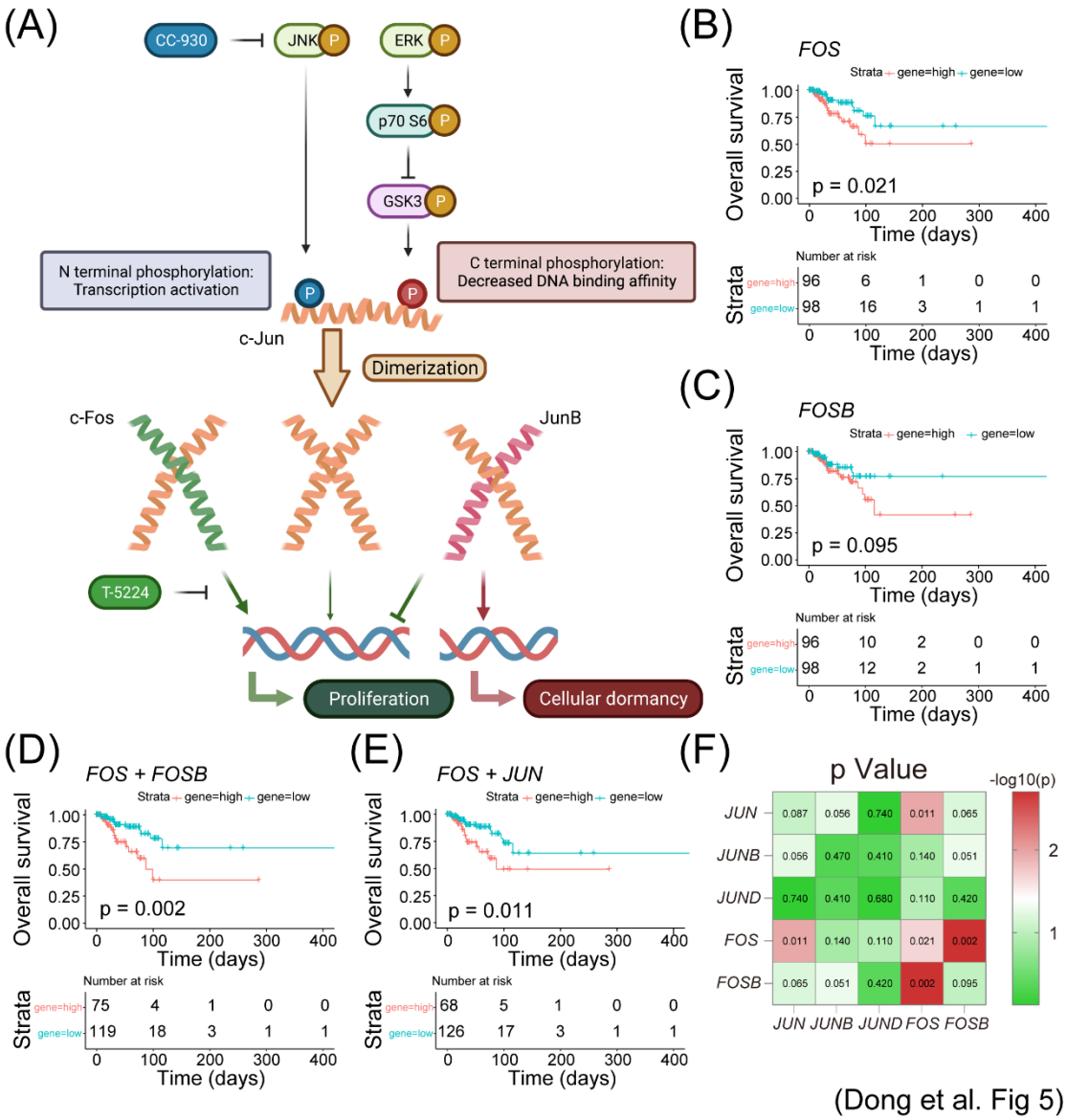

(Dong et al. Fig 5)

Fig 5: AP-1 overexpression was a poor prognostic factor in TNBC

(A) Schematic representation of AP-1 regulation in SCCs. c-Jun is at the center of AP-1 activity. N-terminal phosphorylation site of c-Jun contribute to AP-1 transcription activity, and C-terminal phosphorylation site of c-Jun prejudice to DNA binding affinity. Activation of JNK and ERK contribute to AP-1 transcription activity by phosphorylation of these two sites separately. c-Jun could form homodimer and form heterodimer dimer with c-Fos, promoting proliferation-related gene expression. JunB could from heterodimer dimer with c-Jun, inhibited proliferation-related gene expression through competitive binding, and promoting dormancy-related gene expression such as *CDKN1A* and *GADD45A*.

(B, C) High expression level of *FOS* and *FOSB* was poor prognostic factor for TNBC patients. Patients with

both gene expression > median were considered as high-expression group. Data was acquired from TCGA-BRCA database. n = 111 each, total n =222.

(D) TNBC patient with both *FOS* and *FOSB* high expression had worse prognosis. Patients with both *FOS*/*FOSB* gene expression > median gene expression were considered as high-expression group. Data was acquired from TCGA-BRCA database. n=80, total n=222.

(E) TNBC patient with both *FOS* and *JUN* high expression had worse prognosis. Patients with both *FOS*/*FOSB* gene expression > median gene expression were considered as high-expression group. Data was acquired from TCGA-BRCA database. n=74, total n=222.

(F) The effect of simultaneous high expression of AP-1 gene on the survival of TNBC patients. Patients with two AP-1 subunits gene expression > median gene expression were considered as high-expression group. The data on the diagonal line is the effect of a single gene on patient survival. Data was acquired from TCGA-BRCA database, total n=222.

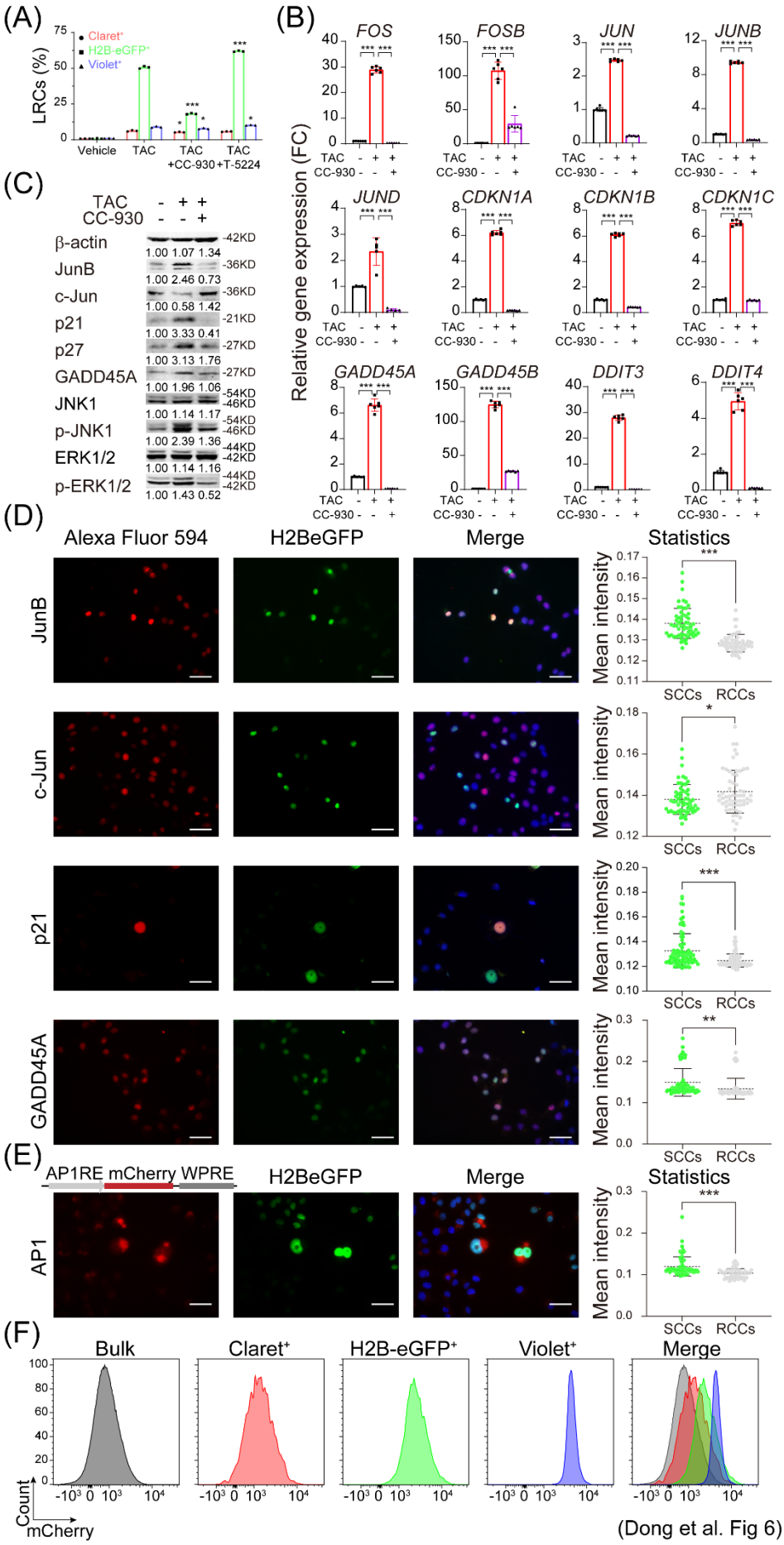

(Dong et al. Fig 6)

992

993 **Fig 6: Mechanisms of AP-1-mediated anti-stress signaling in regulating TNBC SCC properties**

994 (A) CC-930 could reduce SCCs residual caused by chemotherapy in vitro. TAC was a combination of docetaxel,
995 doxorubicin, and cyclophosphamide, with common clinical dosage. Tri-labeled MDA-MB-231 cells were
996 chased for 9 days, and TAC, CC-930 or T-5224 were added to each group. After 3 days of culture cells were
997 collected and analyzed with flow cytometry.

998 (B, C) CC-930 could reduce gene expression and protein level upregulated by TAC treatment. MDA-MB-231
999 cells were treated with TAC and 10 mM CC-930 for 3 days. Relative gene expressions were analyzed by RT-
1000 qPCR (B), and protein level were analyzed by Western Blot (C).

1001 (D) JunB, p21 and GADD45A were enriched in H2B-eGFP^{+} SCCs. Tet-On H2B-eGFP transfected MDA-MB-
1002 231 cells were incubated with doxycycline for 3 days and chasing without doxycycline for 12 days. Cells were
1003 fixed and permeabilized, and stained with corresponding antibody. Scale bar = 20 μm.

1004 (E, F) SCCs were enriched in AP-1 transcriptional activity. Tet-On H2B-eGFP and AP-1 reporter dual
1005 transfected MDA-MB-231 cells were incubated with doxycycline for 3 days and chasing without doxycycline
1006 for 12 days. (E) Cells were fixed and permeabilized, and stained with anti-mCherry antibody. Scale bar = 20
1007 μm. (F) Equal amount of bulk cells, Claret^{+} SCCs, H2B-eGFP^{+} SCCs and Violet^{+} SCCs were collected and
1008 mCherry intensity were analyzed by flow cytometry.

1009 Data are represented as mean ± SD. *$p \leq 0.05$; **$p \leq 0.01$; ***$p \leq 0.001$, Student's t test.

1010

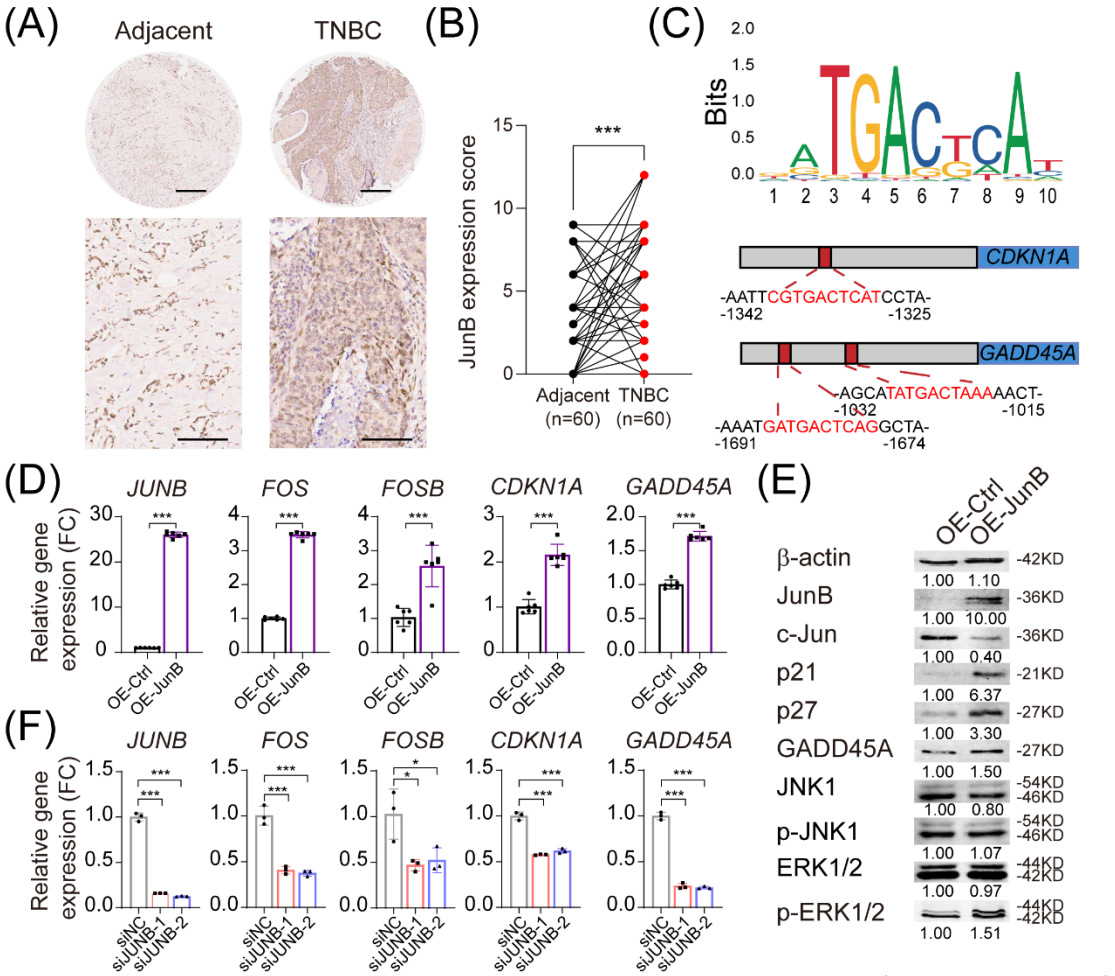

(Dong et al. Fig 7)

Fig 7: JunB was the key regulator of tumor dormancy

(A, B) JunB expression in TNBC patients. TMA with 60 paired tumor adjacent sample and TNBC sample was stained with anti-JunB antibody. JunB expression of each sample was scored and compared pairwise. Scale bar = 300 μm in the upper panel and 100 μm in the lower panel.

(C) Schematic representation of predicted c-Jun/JunB heterodimer binding sites on CDKN1A and GADD45A promoter region.

(D, E) Overexpression of JunB leaded to up regulation of Cip/Kip and GADD45s. Relative gene expressions were analyzed by RT-qPCR (D), and protein level were analyzed by Western Blot (E).

(F) Interfere with JunB would result in down regulation of AP-1 subunits, Cip/Kip and GADD45s. Relative gene expressions were analyzed by RT-qPCR.

Data are represented as mean ± SD. *p ≤0.05; **p ≤0.01; ***p ≤0.001, Student's t test.

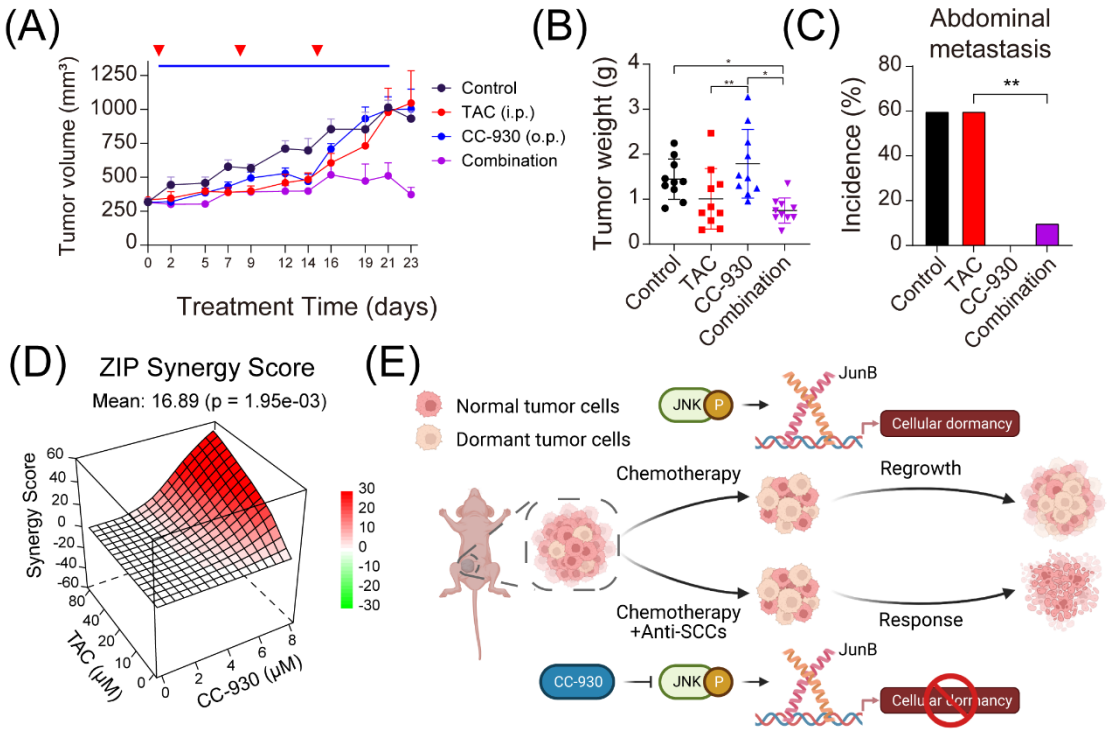

(Dong et al. Fig 8)

Fig 8: CC-930 could reduce SCCs residual after chemotherapy in vivo

(A, B) Timeline of in vivo experiment. MDA-MB-231 cells were injected into forth mammary fat pad in the right flank of nude mice. After 1 week, 40 mice were randomly divided into 4 groups, treated with vehicle, TAC, CC-930 or combination. TAC was given by i.p. every week, and CC-930 was given orally every day. Tumor length (L), tumor width (W) and body weight were measured 3 times a week. Tumor volume was calculated by V = (L x W x W)/2. After 21 days of treatment, mice were sacrificed, and tumors were removed and tumor weights were measured. CC-930 combined with TAC could effectively reduce the tumor volume (A) and tumor weight (B).

(C) CC-930 could reduce abdominal metastasis combined with TAC. n = 10 in each group.

(D) Synergy score of TAC and CC-930. Tumor volume data was annotated as viability data and were loaded into the free software Synergy Finder Plus. Synergy Score was calculated by ZIP synergy scoring.

(E) Dormant TNBC cells were enriched in AP-1 activity and could evade chemotherapy. CC-930 could target the transcriptional activity of AP-1, resulting in more efficient clearance of TNBC.

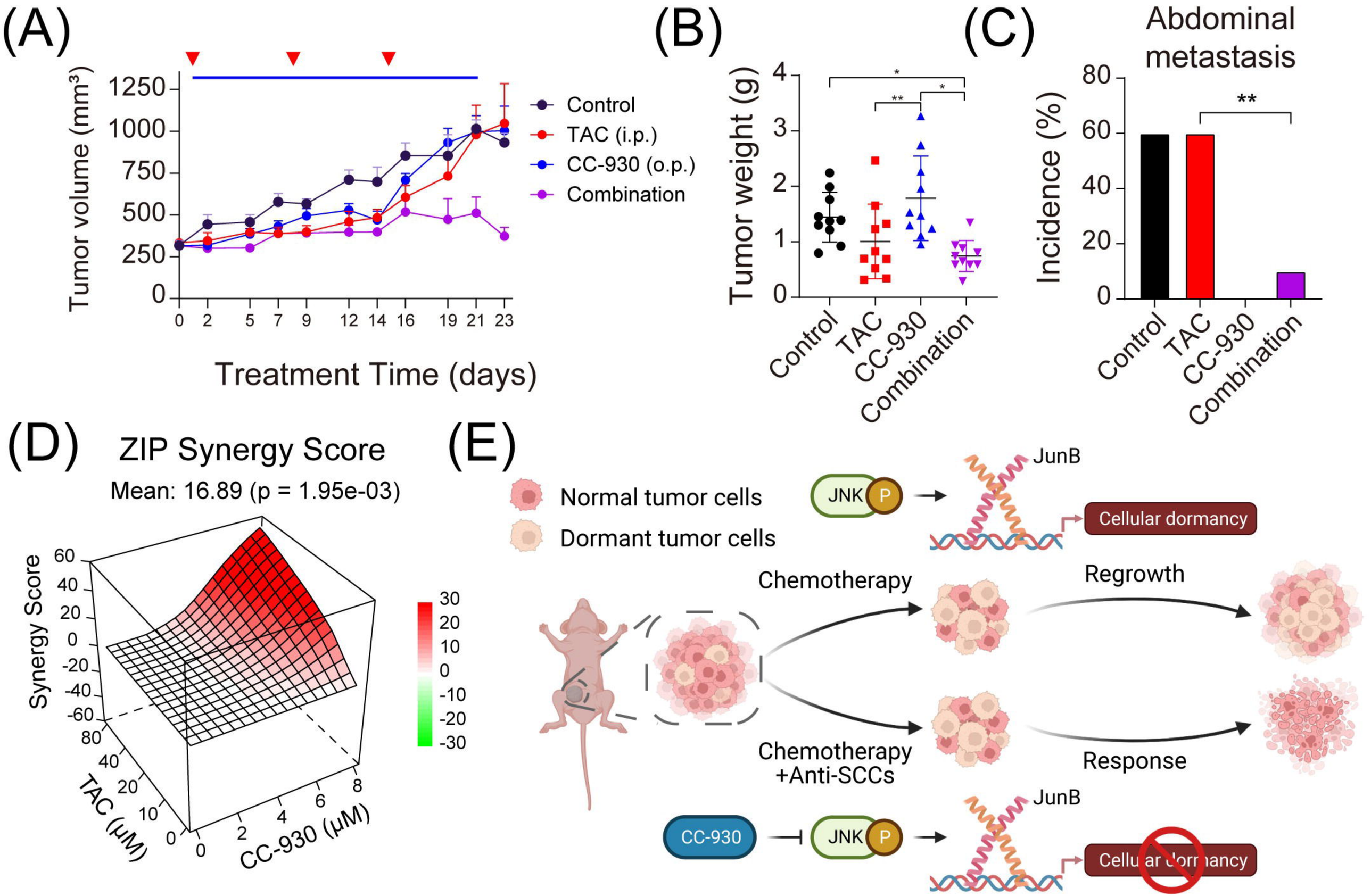

(Dong et al. Fig 8)

(A)

Membrane — Lipid dyes: PKH67, PKH26, Claret

Intracellular — Protein dyes: Blue, Violet, CFSE, Yellow, Far Red

Nuclear histone — H2B-eGFP: eGFP

Name	Ex (nm)	Em (nm)	Channel
PKH67	490	502	FITC
PKH26	551	567	PE
CellVue® Claret	655	675	APC
CellTrace™ Blue	355	410	UV
CellTrace™ Violet	405	450	DAPI
CellTrace™ CFSE	492	517	FITC
CellTrace™ Yellow	555	580	PE
CellTrace™ Far Red	630	661	APC

(B)

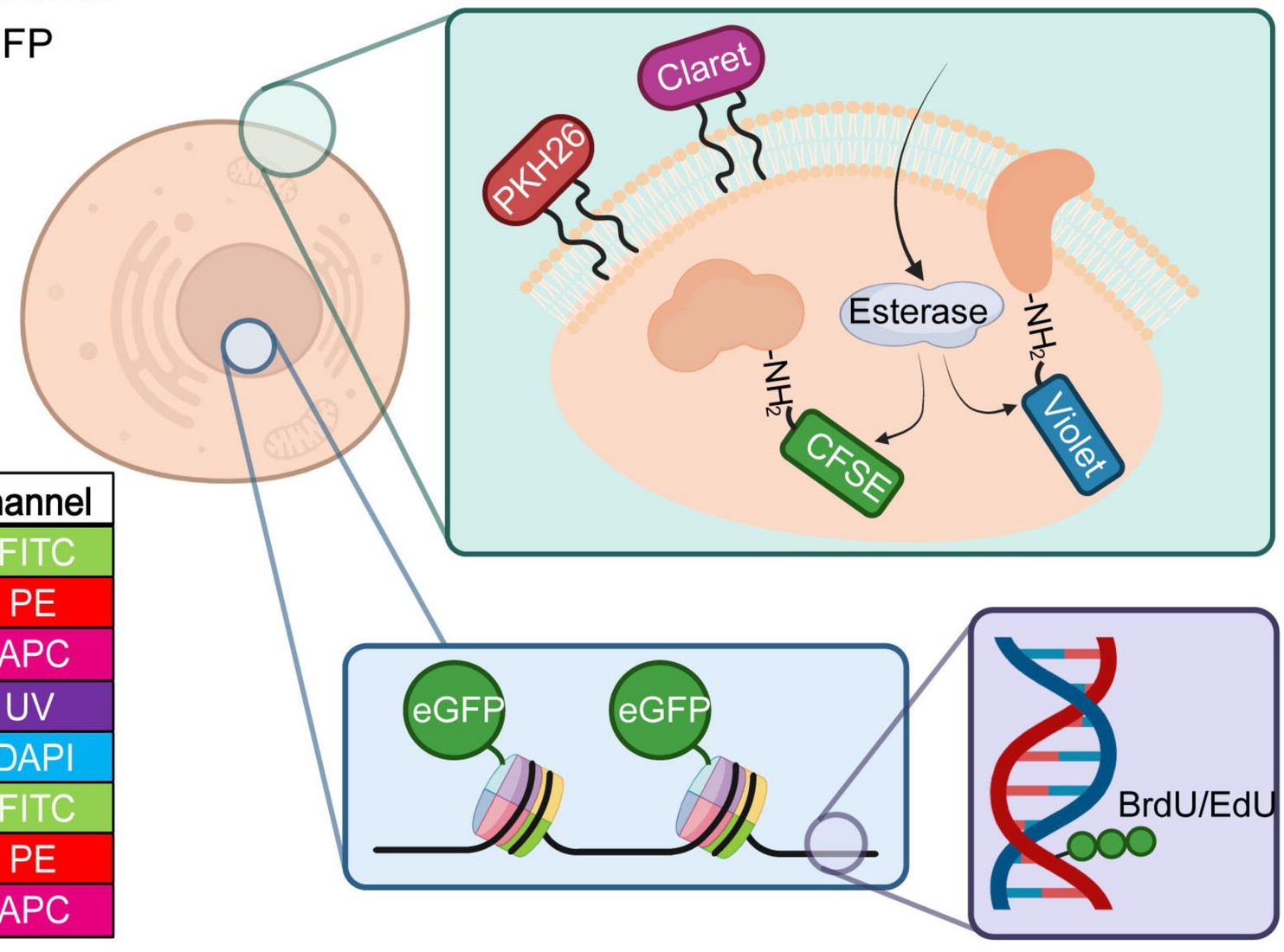

(C)

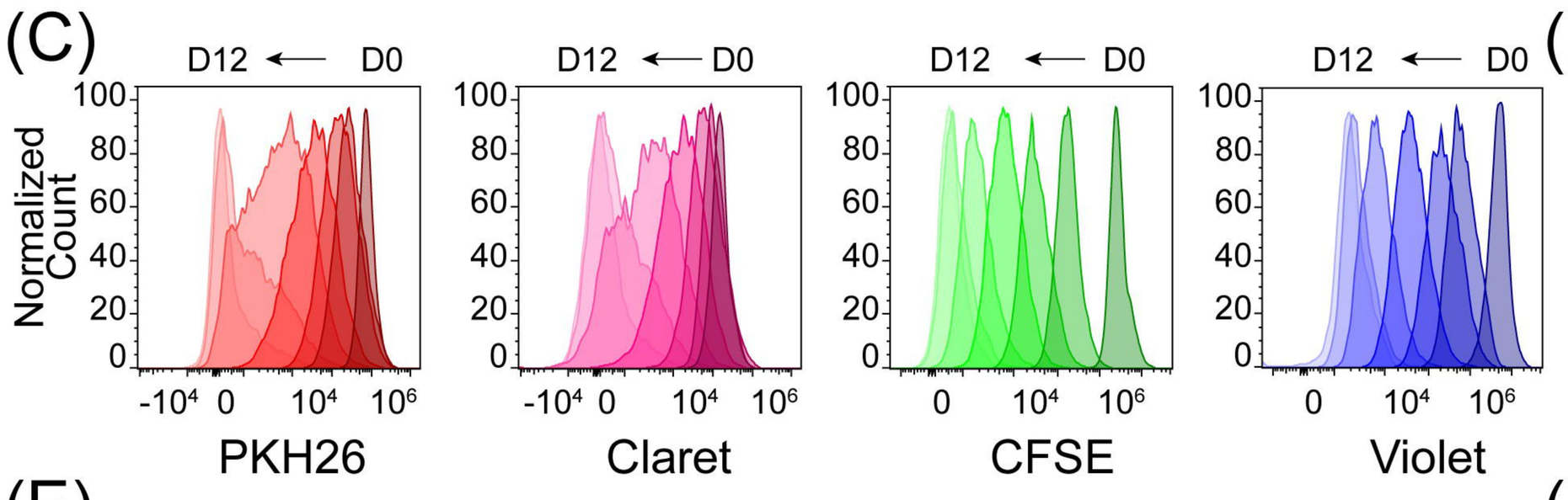

(D)

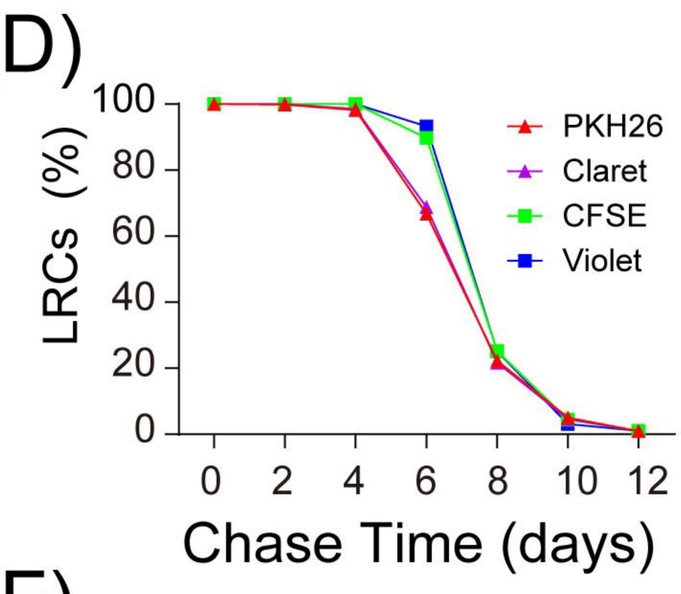

(E)

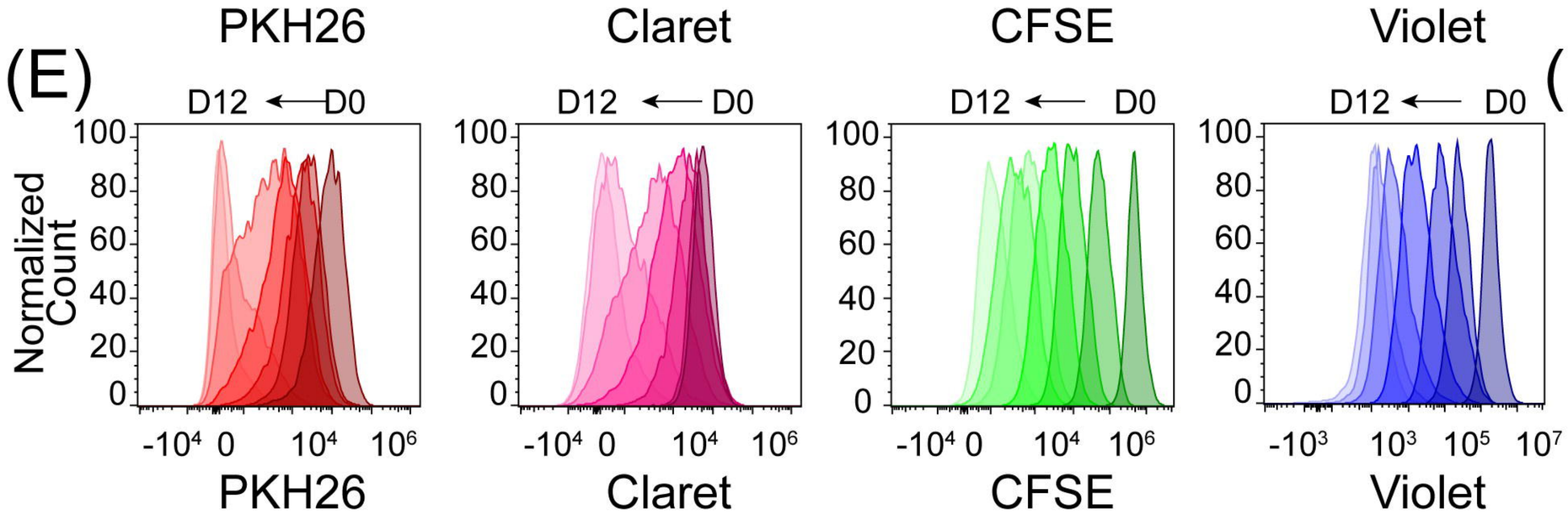

(F)

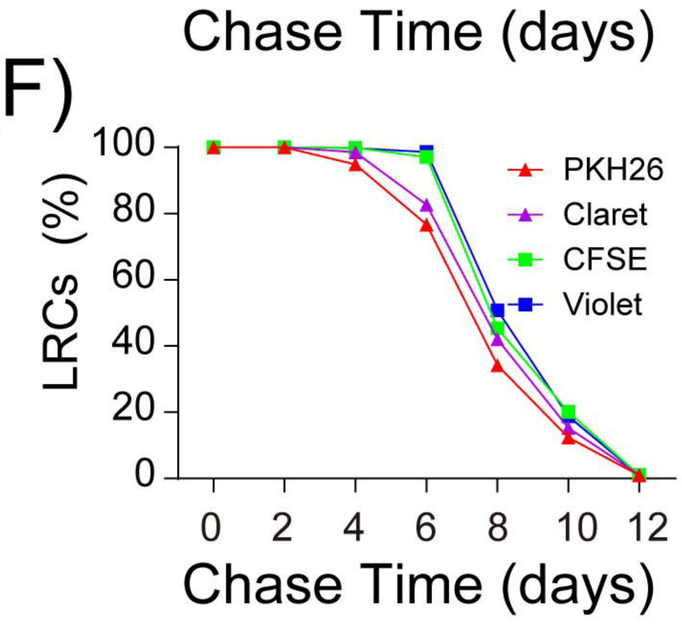

(G)

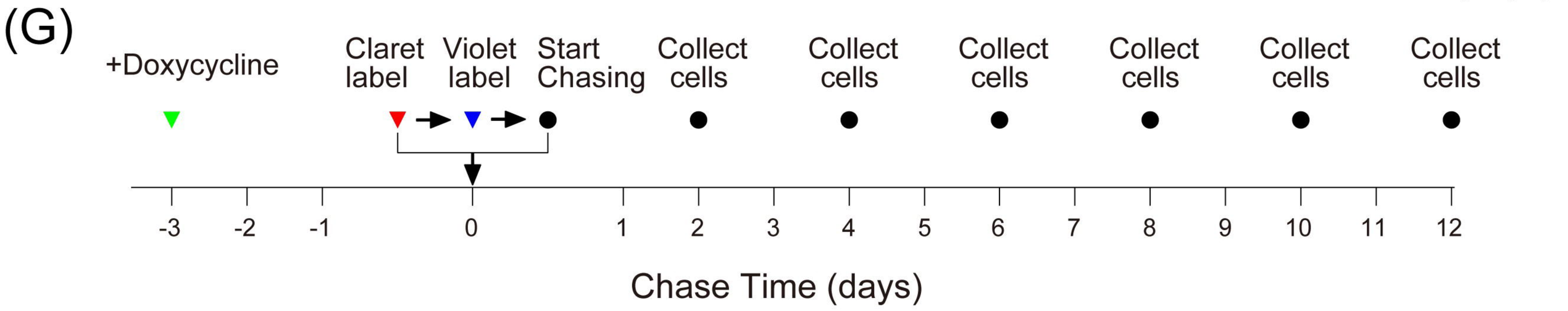

(H)

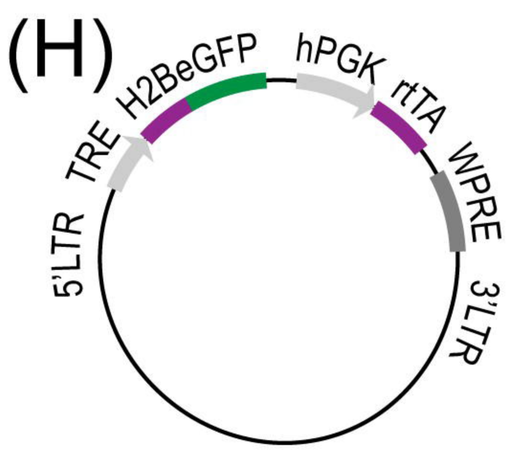

(I)

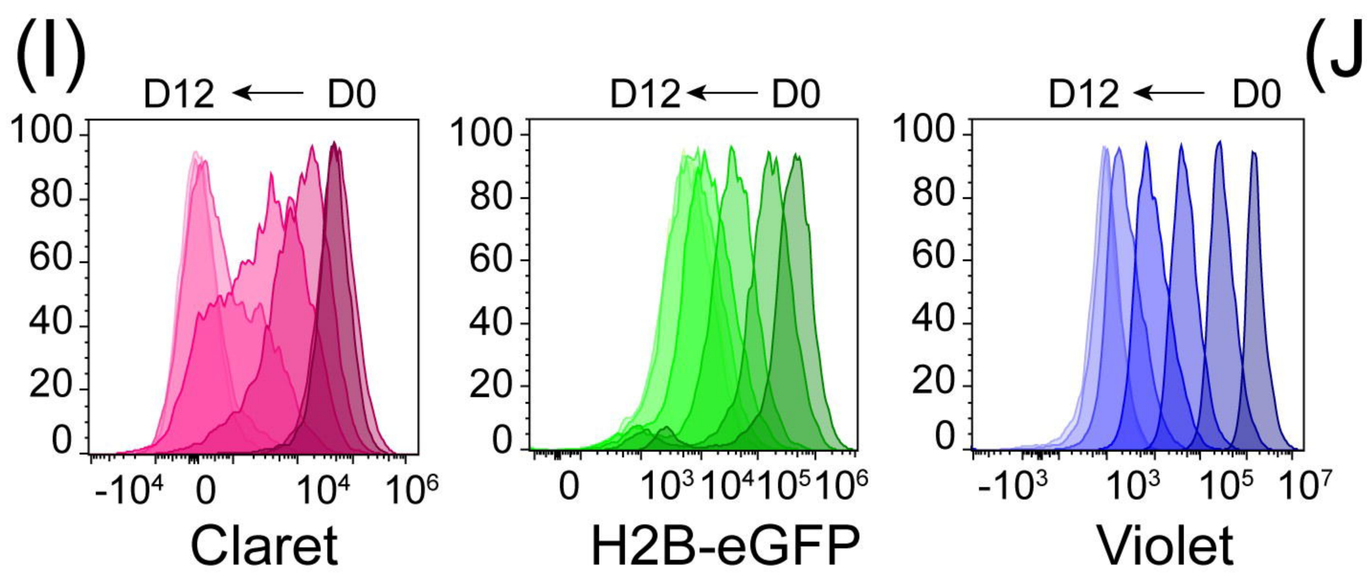

(J)

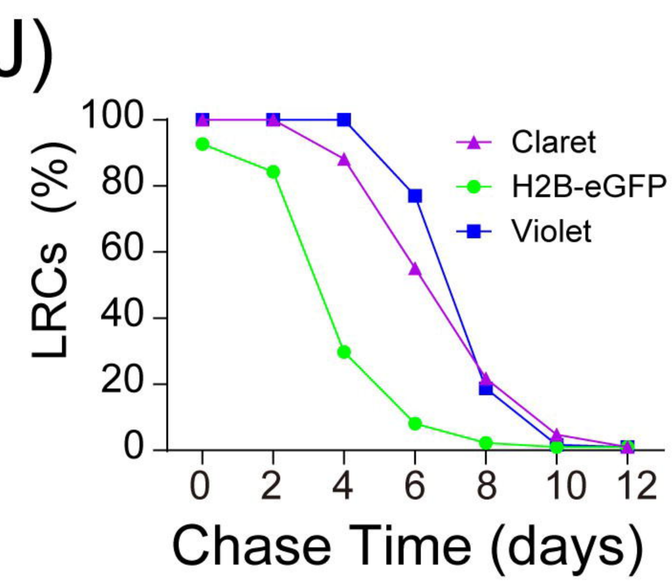

(K)

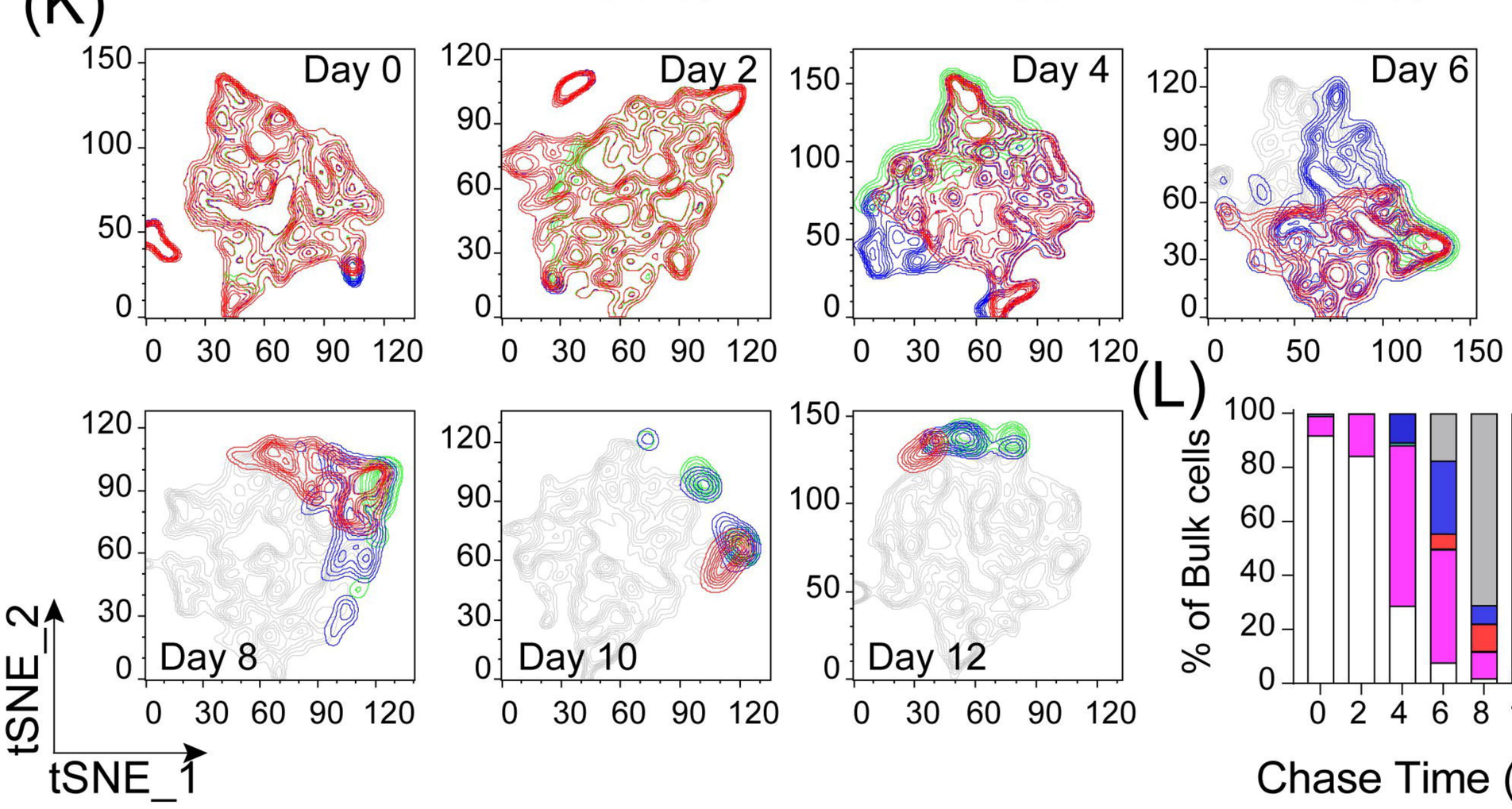

(L)

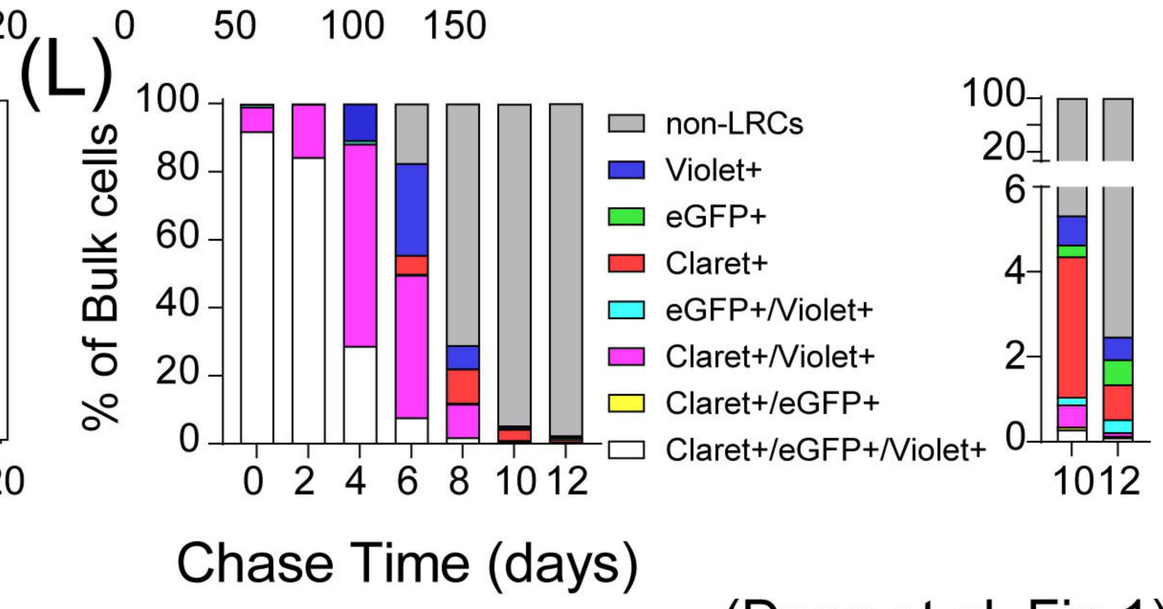

(Dong et al. Fig 1)

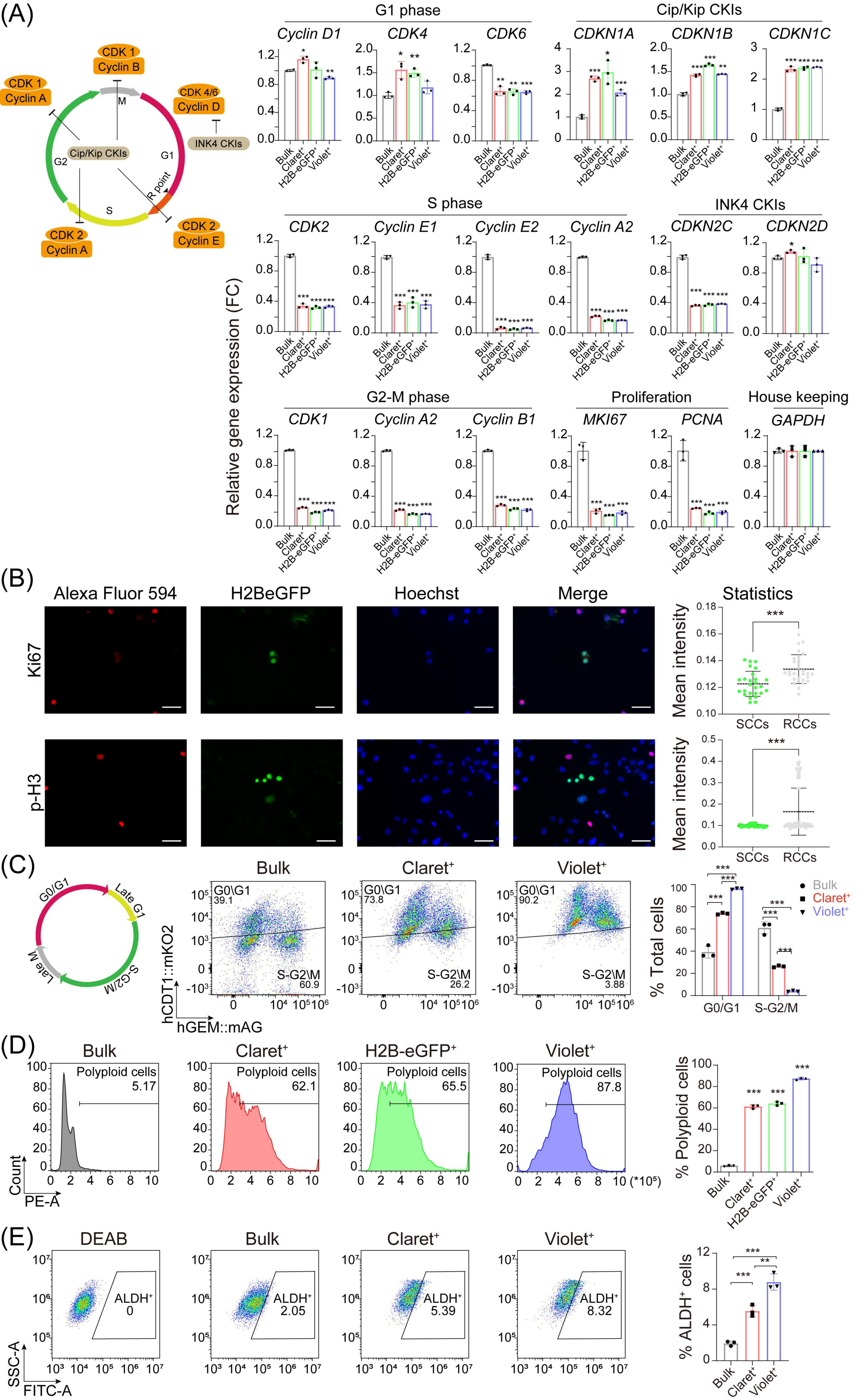

(Dong et al. Fig 2)

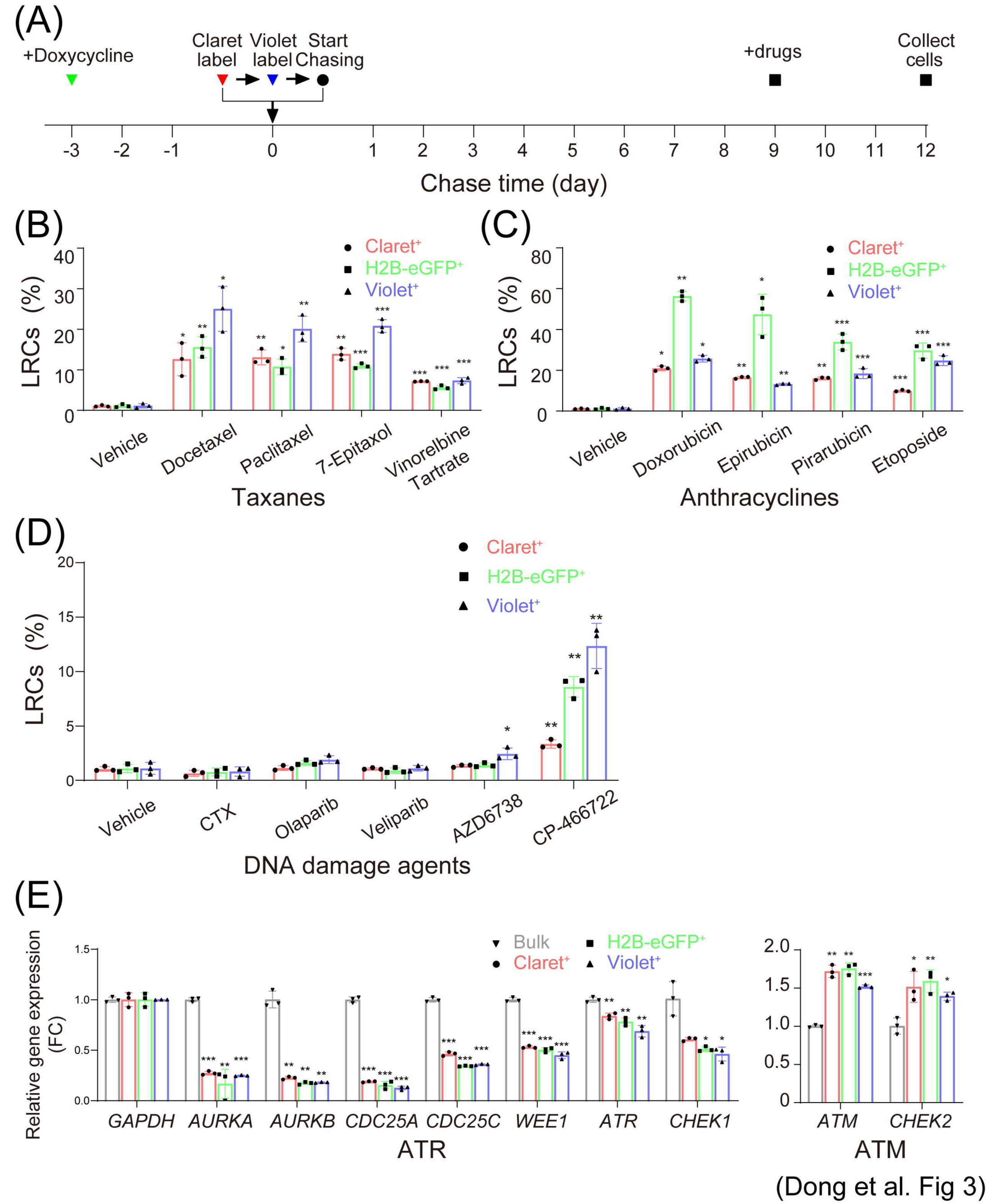
(A)
+Doxycycline
Claret label
Violet label
Start Chasing
+drugs
Collect cells
-3 -2 -1 0 1 2 3 4 5 6 7 8 9 10 11 12
Chase time (day)
(B)
Claret+
H2B-eGFP+
Violet+
LRCs (%)
Vehicle
Docetaxel
Paclitaxel
7-Epitaxol
Vinorelbine Tartrate
Taxanes
(C)
Vehicle
Doxorubicin
Epirubicin
Pirarubicin
Etoposide
Anthracyclines
(D)
Vehicle
CTX
Olaparib
Veliparib
AZD6738
CP-466722
DNA damage agents
(E)
Bulk
Relative gene expression (FC)
GAPDH
AURKA
AURKB
CDC25A
CDC25C
WEE1
ATR
CHEK1
ATM
CHEK2
(Dong et al. Fig 3)

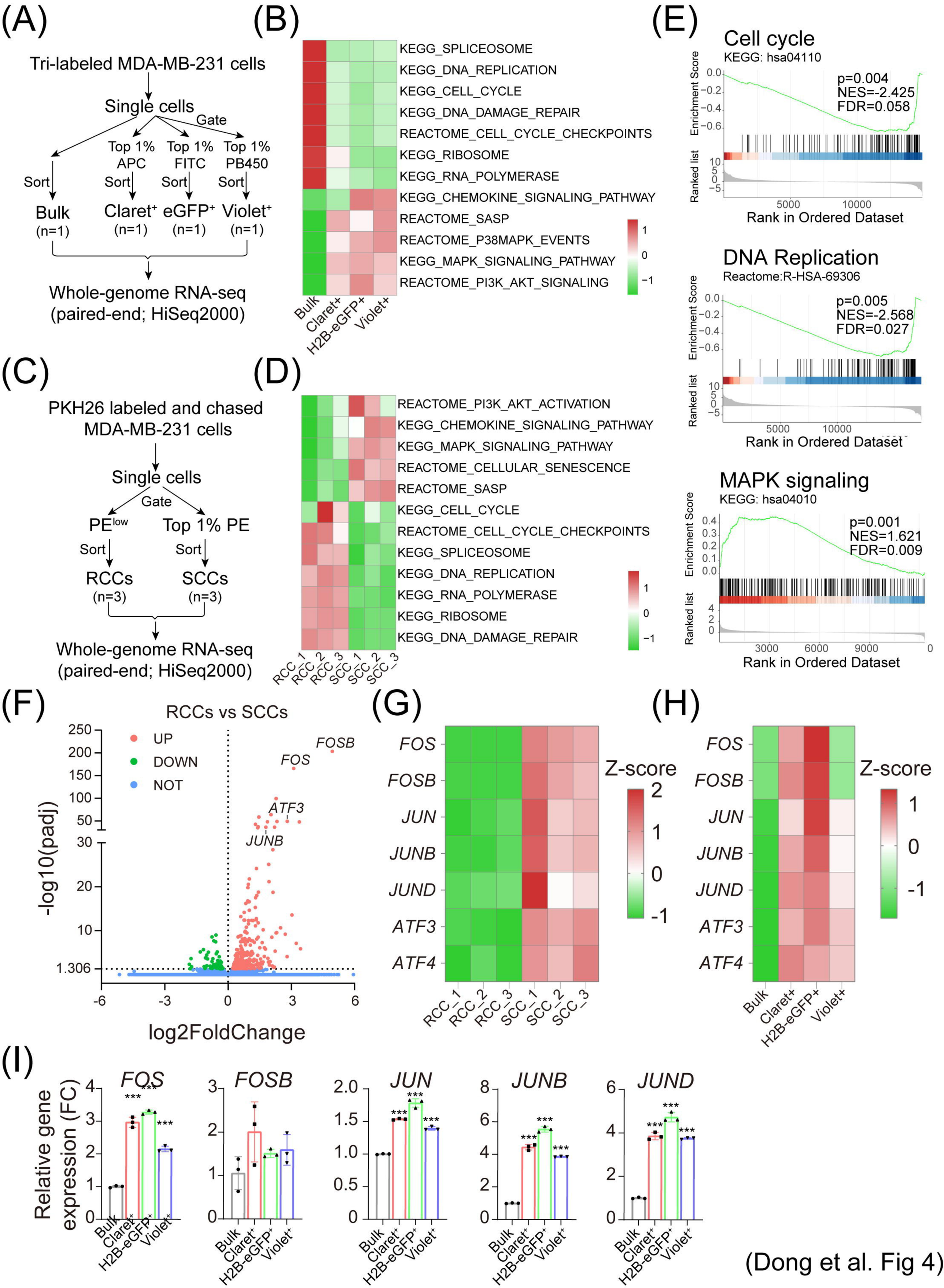

(Dong et al. Fig 4)

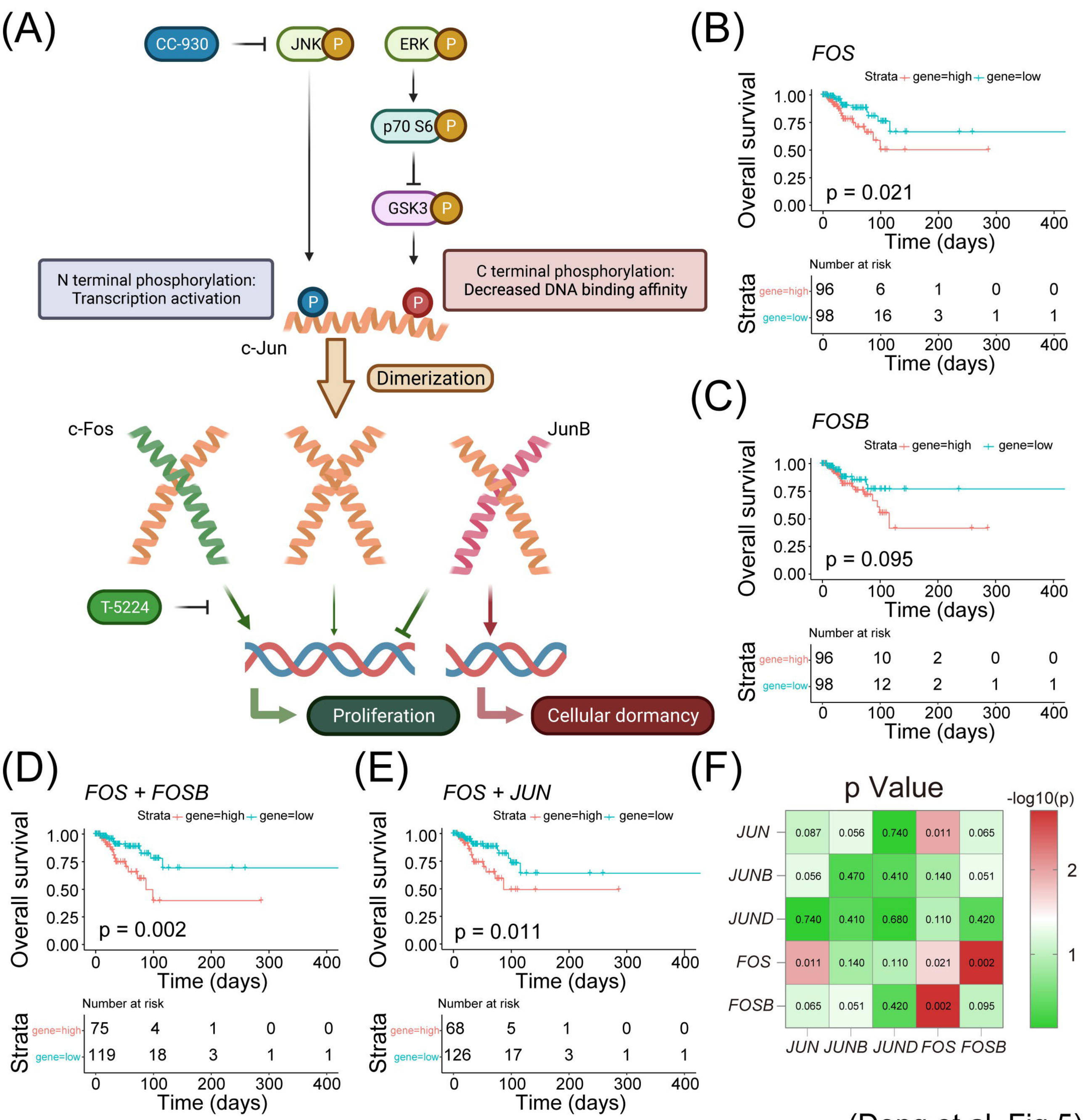

(Dong et al. Fig 5)

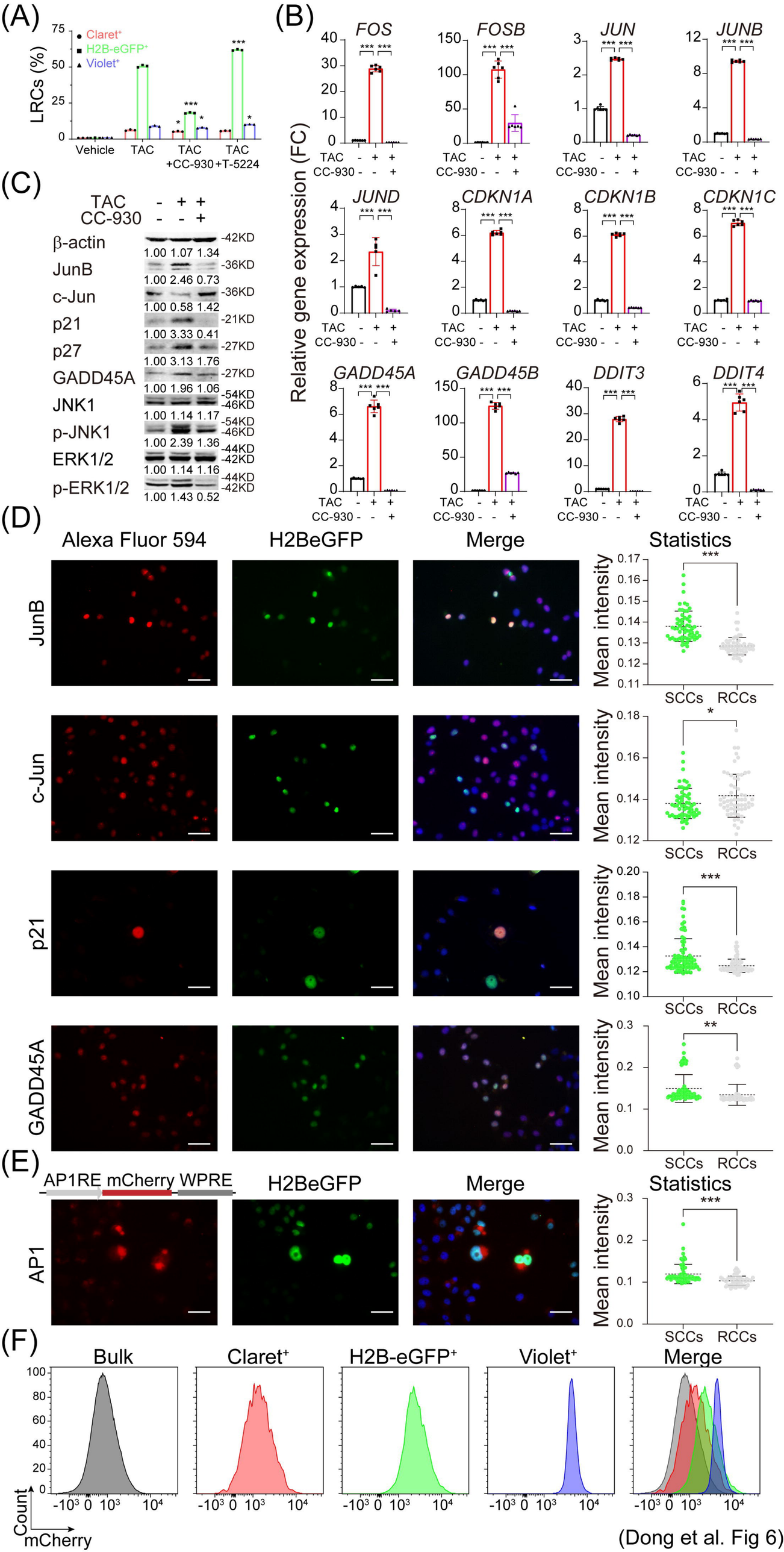

(Dong et al. Fig 6)

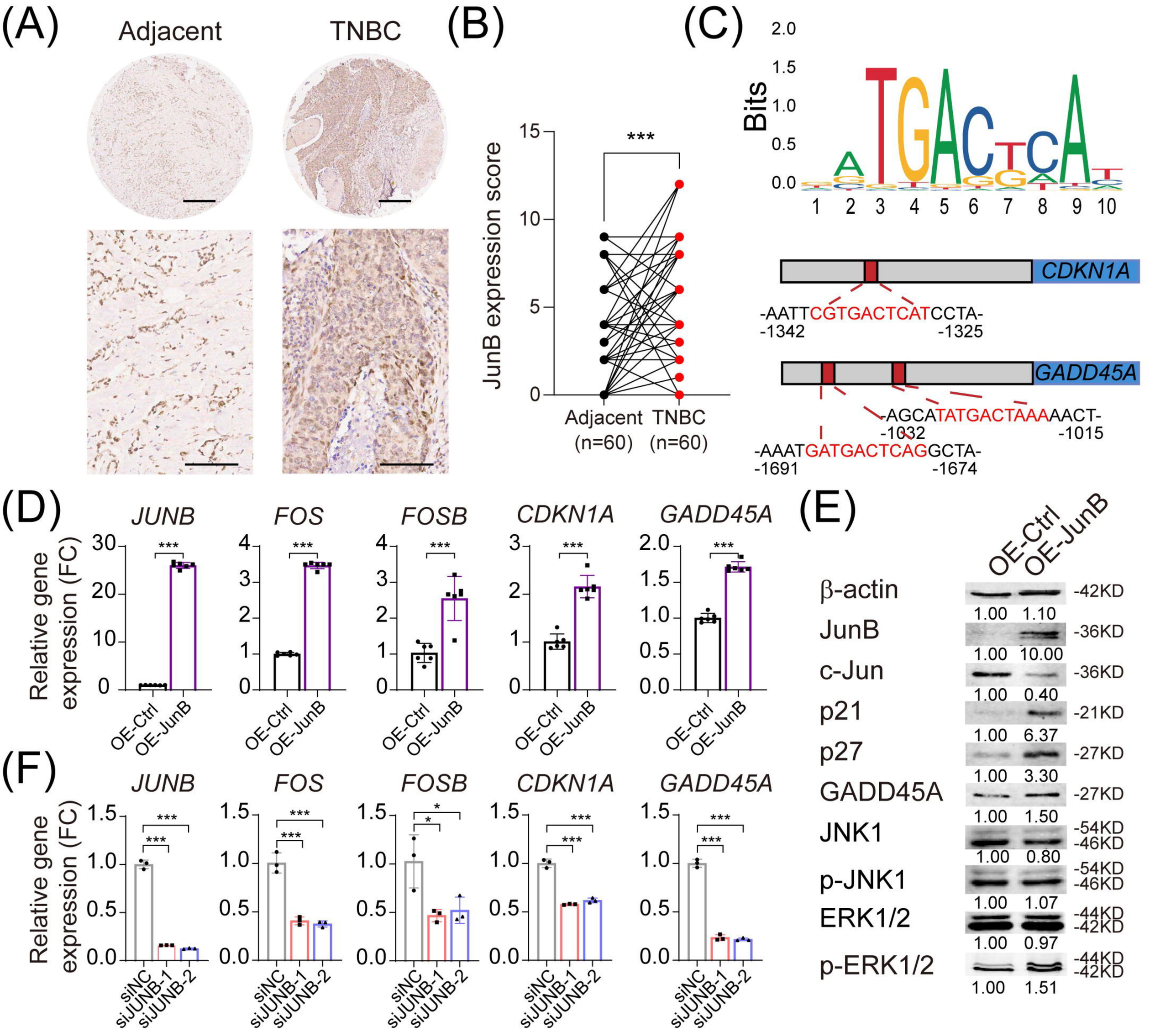

(Dong et al. Fig 7)